Comparisons of VHF Meteor Radar Observations in the Middle Atmosphere With Multiple Independent Remote Sensing Techniques.

Daniel L. McIntosh, BSc. (Hons)

Thesis
submitted for the degree of
DOCTOR OF PHILOSOPHY
at the
UNIVERSITY OF ADELAIDE
School of Chemistry and Physics
Discipline of Physics

August 2009

Chapter 7

Mesospheric Wind Comparisons

7.1 Comparison of Simultaneous Co-located Radar Wind Measurements

Comparisons of both zonal and meridional components of simultaneous wind measurements measured by co-located radar systems will be made. Comparisons are made between VHF meteor radars operating at 33.2 MHz and 55 MHz and a MF radar operating at 1.98 MHz located at Davis Station, Antarctica. Comparisons are also made between the 55MHz meteor radar and 1.98 MHz MF radar at Buckland Park (BP). Previous wind comparisons have been made between MF and meteor winds [Cervera and Reid, 1995, Jones et al., 2003, Tsutsumi and Aso, 2005, Kumar et al., 2007], along with intercomparisons of different MF techniques [Holdsworth and Reid, 2004a,b]. We seek to chiefly compare meteor winds with other co-located independent instruments as well as utilise previous interpcomparisons to gauge the reliability of the comparisons made within this chapter. Comparisons will be made based upon the estimation of statistical parameters including linear regression analysis and estimation of mean difference of velocity estimates. Unlike previous comparisons [Cervera and Reid, 1995, Jones et al., 2003, Tsutsumi and Aso, 2005, Kumar et al., 2007], where there have been at most two independent sources of measurement, Davis and BP locations are unique in that they offer more than two independent sources of measurement. Davis offers wind comparisons between two independent meteor radars and a MF

radar operating in two different modes, O-mode and X-mode. BP offers comparisons between meteor winds and MF winds derived using Spaced Antenna (SA) and Imaging Doppler Interferometry (IDI) techniques.

7.1.1 Regression Analysis

Linear regression analysis using the method of least-squares for examining lines of best fit to data sets which appear to be correlated are well established (e.g. Hocking et al. [2001], Tsutsumi and Aso [2005]). In general the technique is restricted to the case where errors in both sets of data are known. The simplest case would be a set of values $\{v_i\}$ (the independent variable or abscissa) which contain little or no associated error ($\sigma_v = 0$) and a set of measured values (dependent variable) $\{x_i\}$ that has an associated error σ_x. This method has been described in numerous texts such as Taylor [1982] and Bevington and Robinson [1992]. In the case of comparing measurements made by co-located systems, this represents a more complex case in that both measured quantities $\{x_i\}$ and $\{y_i\}$ represent measurements of a common quantity $\{v_i\}$ but also contain some form of intrinsic measurement error, both of which are unknown. Further ambiguity can arise if both techniques measure similar, but not identical, parameters as is the case in comparing meteor and MF winds. As a result, it is possible for there to be differences in wind measurement estimates. Our goal is to be able to obtain a comparison between two sets of data which are assumed to be linearly related to one another with a priori knowledge about the statistical uncertainties associated with either of the two techniques or the associated systems. In practice, the quantities which we measure have a non-zero mean, however we can render our data sets to a zero mean value. The following assumes the mean has been removed from both data sets. The original derivation can be found in Hocking et al. [2001].

We start by describing the measurements made by two different systems as $\{x_i\}$ and $\{y_i\}$ of a common quantity $\{v_i\}$ as follows:

$$x_i = v_i + \delta x_i \tag{7.1}$$

$$y_i = g_0 v_i + \delta x_i \tag{7.2}$$

Where g_0 is a constant but unknown gain factor relative to $\{v_i\}$, and δx_i and δy_i are the associated random noise components. We assume the distribution

of the parameters and their associated errors can be described by a Gaussian probability function $P_G(\mu, \sigma^2)$ with mean μ and variance σ^2 and that the parameters are mutually independant. We describe our intrinsic parameters as follows:

$$v_i \sim P_G(0, \Sigma_v^2), \tag{7.3}$$

$$\delta x_i \sim P_G(0, \sigma_x^2), \tag{7.4}$$

$$\delta y_i \sim P_G(0, \sigma_y^2). \tag{7.5}$$

If we square (7.1) and (7.2) and take an ensemble average we arrive at the following:

$$< x_i^2 >=< v_i^2 > + < \delta x_i^2 >= \Sigma_v^2 + \sigma_x^2, \tag{7.6}$$

$$< y_i^2 >= g_0 < v_i^2 > + < \delta y_i^2 >= g_0^2 \Sigma_v^2 + \sigma_y^2. \tag{7.7}$$

We have assumed that v_i, δx_i and δy_i are uncorrelated quantities and as such the averages over the crossed-product terms are zero. If we multiply (7.1) and (7.2) we also obtain:

$$< x_i y_i >= g_0 < v_i^2 >= g_0 \Sigma_v^2. \tag{7.8}$$

We now replace the ensemble-averaged quantities of the measured data with sample expectations; i.e. $< x_i^2 >$ is replaced with $\eta_x^2 = \sum_i x_i^2/N$, $< y_i^2 >$ with $\eta_y^2 = \sum_i y_i^2/N$ and $< x_i y_i >$ with $\eta_{xy} = \sum_i x_i y_i$. We also consider the "non-noise" quantities $\{v_i\}$ to essentially be the "signal" embedded within the our data. We apply the following definitions and recognise that Σ_x^2 and Σ_y^2 represent the variances of the signal components of the measured quantities $\{x_i\}$ and $\{y_i\}$; i.e.

$$\Sigma_x^2 = \Sigma_v^2, \tag{7.9}$$

$$\Sigma_y^2 = g_0^2 \Sigma_v^2. \tag{7.10}$$

If we combine (7.6) and (7.7) along with our definitions for η_x^2, η_y^2 and η_{xy}, we obtain two key expressions which tells us that the variance of each data set is given by the sum of the signal variance and the random noise variance

$$\eta_x^2 = \Sigma_x^2 + \sigma_x^2, \tag{7.11}$$

$$\eta_y^2 = \Sigma_y^2 + \sigma_y^2. \tag{7.12}$$

Likewise we have

$$\eta_{xy} = g_0 \Sigma_x^2. \tag{7.13}$$

We need to relate these results to those obtained via regression analysis techniques. As mentioned earlier, it is usually common practice in regression analysis to assume one of the parameters contains no error, while the error is entirely associated with the other. One typically might assume a case where $\sigma_x = 0$ and that all the error is associated with variable y_i. This is of course untrue for our data sets, but it does however provide us with a starting point when comparing the data sets. In actual fact, when trying to determine the slope of the line of best fit to the scattered data, the results obtained when assuming one parameter ($\sigma_x = 0$) contains no error and vice versa represent the bounding limit cases of the analysis. If we take (7.11) and (7.13) along with our assumption of $\sigma_x = 0$ and solve for the value of g_0, we then obtain an estimate for the slope of the line which we denote by g'_x and is given by

$$g'_x = \frac{\eta_{xy}}{\eta_x^2} = g_0 \frac{\Sigma_x^2}{\Sigma_x^2 + \sigma_x^2} \leq g_0. \tag{7.14}$$

We recognise this result as being the same as that derived in many standard texts as the slope of the regression line obtained using the method of least squares; i.e. the regression of y on x [Bevington and Robinson, 1992]. The resulting regression line has the form

$$y_i = g'_x x_i + c, \tag{7.15}$$

where c is a constant.

Similarly, we apply the same method of solving for g_0 this time with the assumption $\sigma_y = 0$ and using (7.12) and (7.13). This yields the result of the regression of x on y, which obeys the equation

$$x_i = \frac{1}{g'_y} y_i + d \tag{7.16}$$

viz.

$$g'_y = \frac{\eta_y^2}{\eta_{xy}} = \frac{1}{g_0} \frac{\Sigma_y^2 + \sigma_y^2}{\Sigma_y^2} \geq g_0. \tag{7.17}$$

Note in this case we have used an inverted form for the slope (i.e. $1/g_y$) such that our regression equation takes the form

$$y_i = g'_y x_i + d', \tag{7.18}$$

where d and d' are constants.

As mentioned previously, these two estimates represent limiting values for g_0 and thus provide good starting points for determining a better estimate for g_0. Values for g'_x and g'_y are easily found with most analytical software packages (remembering that the result for the slope of the least-squares line produced from the regression of x on y requires inversion in order to be consistent with the the definition we have used for g'_y). Provided that we have a large enough sample size, the estimates of $g_x =< g'_x >$ and $g_y =< g'_y >$ will be valid representations of the population values.

Finally, equating (7.14) ($\eta_{xy} = g_x \eta_x^2$) and (7.13) ($\eta_{xy} = g_0 \Sigma_x^2$), applying (7.11) and eliminating η_x^2 yields the following result

$$\frac{\sigma_x}{\Sigma_x} = (\frac{g_0}{g_x} - 1)^{1/2}. \tag{7.19}$$

Similarly,

$$\frac{\sigma_y}{\Sigma_y} = (\frac{g_y}{g_0} - 1)^{1/2}. \tag{7.20}$$

Furthermore, we can use (7.11) and (7.12) to write

$$\sigma_x = \eta_x (1 - \frac{g_x}{g_0})^{1/2}, \tag{7.21}$$

$$\sigma_y = \eta_y (1 - \frac{g_0}{g_y})^{1/2}. \tag{7.22}$$

By employing the technique of Holdsworth and Reid [2004a], both the sample variances η_x^2 and η_y^2 can be obtained by calculating the Root-Mean-Square

(RMS) error between contiguous points in each data set $\{x_i\}$ and $\{y_i\}$ using the following equation

$$\eta = \sqrt{\sum_{i=1}^{M} \frac{(a(t+1) - a(t))^2}{2M}}. \tag{7.23}$$

This will help restrict the range of possible measurement errors [Holdsworth and Reid, 2004a]. The only unknown quantities above in (7.21) and (7.22) are g_0, σ_x and σ_y. These quantities are uniquely inter-related and as such, the specification of one allows the immediate determination of the other two. It is of importance to note that both σ_x and σ_y are not without bounds, in fact they take their maximum values $(\bar{\sigma_x}, \bar{\sigma_y})$ when the other is assumed to be zero. This was the limiting case discussed earlier we used to solve for g_x and g_y; i.e. $\sigma_x = \bar{\sigma_x}$ when $\sigma_y = 0$ and $g_0 = g_y$ and vice versa. We may also plot a graph of $g_0(\sigma_x, \sigma_y)$ with an assumed abscissa $\sigma_x = 0, ..., \bar{\sigma_x}$ which shows the relationship of all three parameters. See Figure 7.3. This enables a set of possible values for g_0 based upon estimates of σ_x and σ_y graphically. In all of the comparisons to follow the only data points included were those in which both data sets contained valid estimates of the wind field and each of the records contained a zero error flag. For a description of error flags associated with ATRAD systems see Holdsworth and Reid [2004a] and Holdsworth et al. [2004]

7.1.2 Interpretation of σ_x and σ_y

We need to consider the true meaning and significance of σ_x and σ_y. When we use two instruments to measure the same quantity, both of these variables tell us what the associated measurement error for each technique is. While in some cases, such as the comparison of winds from two different meteor radar systems, we are in essence measuring the same geophysical phenomena (assuming both radars are using the same meteors to estimate the wind field), there are cases such as the comparison of MF and Meteor derived winds that use different geophysical phenomena to obtain their estimates; i.e. meteor trails and electron density gradients induced by solar radiation and turbulent mixing. The ideal scenario would be to measure the exact same region of space, over the same time interval, and with the 33.2 MHz and 55 MHz meteor systems at Davis this is possible. Due to the interleaved

operation of the 55 MHz Meteor system with the ST operations, measuring of the same time interval 100% of the time is not quite possible. The difference in the peak of the height distribution of echo detections is only 2 km, with both height distributions displaying similar widths. See Figure 7.19. As such any statistical weighting effect the meteor distribution may have upon observations by both meteor systems over the height region of interest can be considered to be the same. The key point to note is that both σ_x and σ_y not only reflect the intrinsic measurement errors of each system, but also contain information about how "different" the two techniques are [Hocking et al., 2001]; i.e. different frequency of observation in the meteor-meteor case or meteor-MF SA comparison or meteor-MF IDI comparison. In the case of the comparisons between meteor systems, the error associated with the difference between the two techniques should be quite small in comparison to the measurement error. When applying the results of the regression analysis to the two sets of data to be compared, the least-squares fitting procedure makes the assumption that there is a technique which is not the same as either of the techniques applied to obtain the data sets. In essence it assumes that there exists a technique which represents a compromise between the techniques used by each system and that the systems themselves are attempting to utilise this technique [Hocking et al., 2001]. Thus when interpreting the results for σ_x and σ_y from the regression analysis, we need to acknowledge that these values describe both the measurement error and the natural spatial and temporal variations associated with the medium and the quality of the experiment being used to perform the measurements.

There is also an alternative means of interpreting σ_x and σ_y. One could view the result as having two components, one being fully correlated between the two techniques and the other component corresponding to an uncorrelated component. This would imply that the correlated component would correspond to the the similar features which are present in both data sets, while σ_x and σ_y represent the contribution of each technique to the uncorrelated component. In the case of the meteor comparisons where the measurement technique can be assumed to be the same, this will give us a direct indication of the error associated with the experiment, i.e. running it as a part of a sequence which contains ST experiments, along with the detection of echoes and wind estimates at differing frequencies. This should provide us with a true estimate of the system error which should enable us to obtain a better estimate of the relative error between two different techniques.

7.2 Davis 33.2 MHz and 55 MHz Meteor Wind Comparisons

Davis is quite unique in that it has two co-located meteor radar systems. Both radar systems make use of interferometric techniques for meteor observations. The main differences between the two systems are the operational frequencies and the experimental sequence configured on both radars (refer to section 3.1.10). The 33.2 MHz system continuously operates a sequence with only a single meteor experiment while the 55 MHz system continuously operates a sequence of multiple experiments comprising of meteor, Polar Mesospheric Summer Echoes (PMSE) and ST experiments. This mode of operation for the 55 MHz meteor system is discussed later as a potential source of error. In essence both systems use the same technique for generating wind estimates which implies that the source of error due to the technique itself should not influence the linear relationship between the two measured sets of data. Wind estimates from both systems are compared based upon the estimation of statistical parameters along with linear regression analysis. Ideally a 1:1 relationship should exist between the measurements of both systems, i.e. all data points lay on a line "$y = x$", however this is not quite the case. Sampling of winds using possibly different meteor trails in a particular time-height bin, different experimental sequences used in the operation of both radars along with system error contribute to the observed scatter in Figure 7.1. The co-location of both instruments provides a unique opportunity to better understand and characterise the differences observed between commonly measured parameters which are measured in an almost identical manner by two similar systems.

We begin by producing scatter plots for each component of the wind vector for each height bin (e.g. Figure 7.1). We observe that there is a strong linear relationship between the two sets of data, however the data points are scattered about the 1:1 relationship (the red line in Figure 7.1). We therefore apply the technique in Section 7.1.1 in order to deduce what the true relationship between the two data sets is; i.e. g_0 and subsequently the uncertainties associated with each set of measurements. If we apply regression techniques using the method of least-squares, firstly the regression of y on x and subsequently the regression of x on y, we generate two slope estimates for the line of best fit to the data (red and blue lines in Figure 7.2 respectively). Neither of these lines are correct fits to the data as the least-

squares-fit analysis assumes that one set of data contains no error. However, as mentioned in Section 7.1.1, they do provide us with a starting point from which we can attempt to estimate the true slope of the line of best fit to the data. As can be seen from the form of the expressions in (7.21) and (7.22) we have 2 equations with 3 unknown quantities. This makes determining a value for g_0 analytically not possible unless we either have more information about the error in one set of measurements or we can assume the error associated with the noise quantities of both sets to be equal; i.e. $\sigma_x = \sigma_y$. In the event we make the assumption that both sets of measurements contain equal noise error, then we can calculate a value for the true slope estimate g_0 (plotted as the green line in scatter plots) and subsequently determine the values for σ_x and σ_y. In the case where we can't assume $\sigma_x = \sigma_y$, then the only means of determining possible values for the three quantites is to plot the relation between the three unknown parameters, as can be seen in Figure 7.3. From the plot we are then able to determine possible values for g_0 and subsequently σ_x and σ_y.

The data was grouped into year long data sets for 2005, 2006, and 2007. The winds were hourly averaged estimates of the zonal and meridional components of the wind field that had an associated "error flag=0" tag (see Table 2.1). The results of applying the analysis technique to the winds over the height range are illustrated more clearly by Figures 7.4, 7.5, and 7.6 for 2005, 2006 and 2007 respectively. If we first consider the correlation results in Figures 7.4, 7.5 and 7.6 we can see that there is a higher correlation between the two systems with the meridional component of the wind compared with the zonal component. The zonal component correlations show a more consistent result over the height range compared with the meridional component correlations. This is a consistent result over the three years of observations. It was initially thought that this was the result of using linear receive antennas on the meteor radar systems as the polar diagram for the receive antennas is non-isotropic (see Figure 7.7). The antenna gain results are shown for 45° and 60° from zenith as the majority of the meteor flux is found in that zenith angle range (see Figure 7.8). It was later found that the antennas were aligned (end-fire) in the NE-SW direction which implied that both zonal and meridional directions share equal maximum and minimum gain. Depending upon the variation in azimuth of the flux of the meteor stream, there could still be a bias introduced into the wind estimates depending upon the preferential direction of the stream (see Figure 7.9). This could be verified with

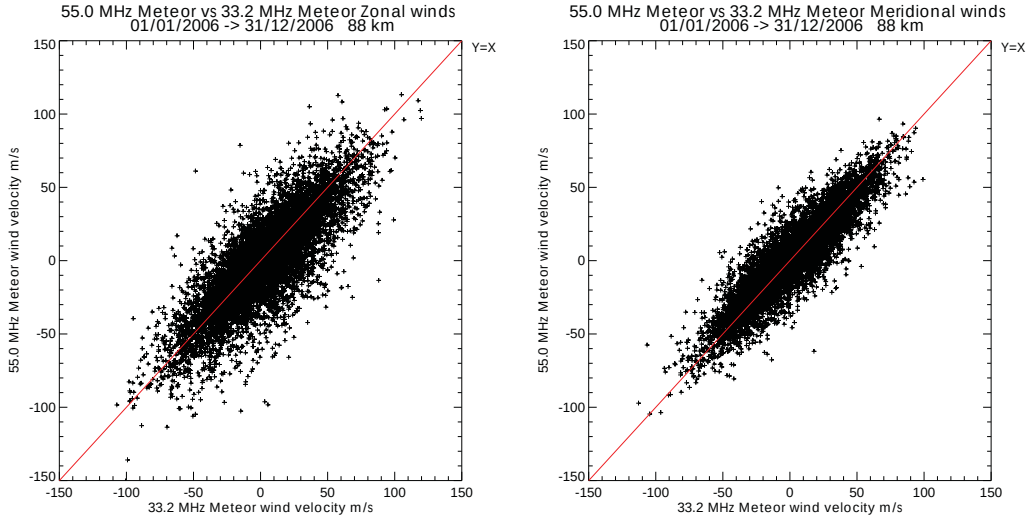

Figure 7.1: Example of scatter plot used to compare 33.2 MHz and 55 MHz meteor radar wind estimates from Davis station. Each velocity estimate represents an hourly averaged wind velocity by the radar. All "error code=0" (see Table 2.1 for descriptions) wind estimates from both radars during 2006 are represented. The red line indicates the ideal linear relationship. Each '+' symbol represents an hourly averaged wind velocity measurement in the above and subsequent scatter plots.

more current data as the receive antennas on the 33.2 MHz radar have been replaced by crossed dipole antennas similar to the Darwin system which have circular polarisation capability and thus a more isotropic radiation pattern. This means any observed bias in azimuth direction of the meteor flux observed in the data is real and not a product of the variation in azimuthal gain of the antenna and the meteor flux.

The mean ratios (Y/X) for the zonal and meridional components of the 55 MHz to 33.2 MHz systems were calculated for each height bin using an outlier rejection scheme with a 2.5 standard deviation rejection criteria and only where X≠0. This suggests that either the 55 MHz is underestimating or the 33.2 MHz is overestimating the wind components and the effect is more prevalent in the zonal direction. As to which case it is, we can not definitively say at this point. Hocking and Thayaparan [1997] showed that least-squares solutions using a small number of echoes can lead to suspect wind estimates.

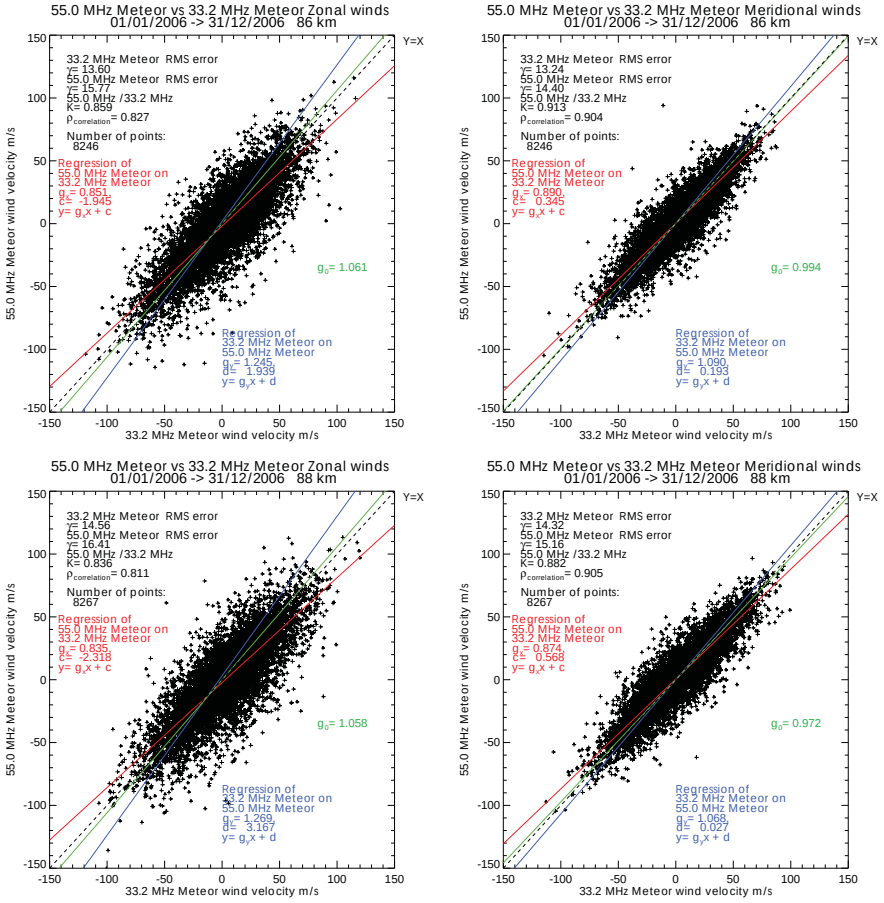

Figure 7.2: Scatter plots with regression analysis results. Here we have examples of scatter plots from two consecutive heights comparing zonal and meridional wind velocity estimates. The red line is the slope to the linear fit when performing the regression of the 55 MHz data on the 33.2 MHz data. In this case it is assumed that the 33.2 MHz velocity data set contains no errors and that all errors can be attributed to the 55 MHz data set. The blue line is the result when making the reverse assumption where the 33.2 MHz data is assumed to contain all the errors and the 55 MHz is assumed to contain no errors. Both of these lines form a bounding region to where the true slope of the line is. The green line is the slope of the scatter when both techniques are assumed to contain equal error. We can clearly see that this is a very good assumption for the meridional winds, but not quite as good for the zonal winds. The meridional green line slope differs from 1.0 by $\sim$0.7% where as the zonal differs by $\sim$6%.

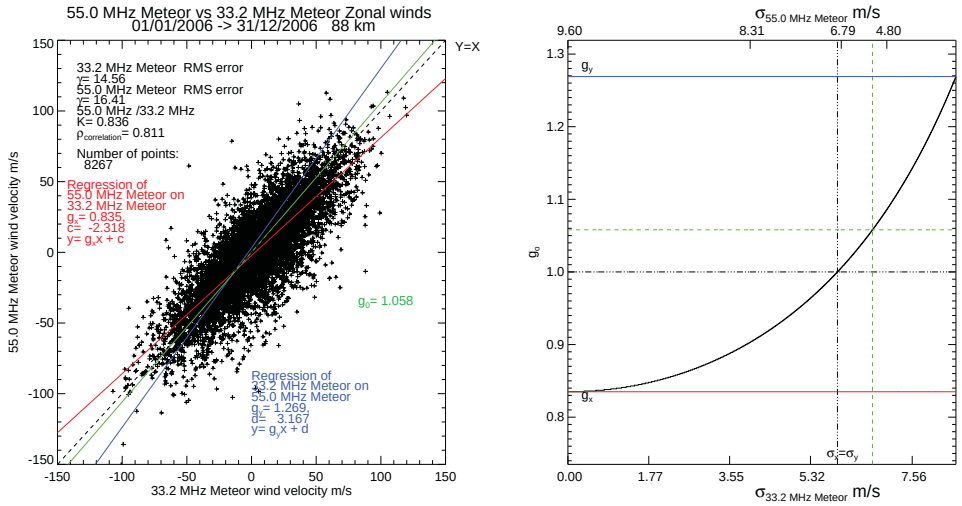

Figure 7.3: Scatter plots with graphical solution for σ_x, σ_y and g_0. The curve is bounded by the results of the regression fits and hence shows the upper limits on the error quantities associated with the random noise variances. The horizontal blue and red lines in the second plot show the bounded region of possible solutions for g_0 that are determined by g_x (red solution) and g_y (blue solution) from the first plot.

It is known that the echo detection rate over the height range and through the year is much less for the 55 MHz system than the 33.2 MHz system (see Figure 7.19), this would suggest according to the findings of Hocking and Thayaparan [1997] that the 55 MHz system would be more likely to produce suspect wind estimates. The observed mean ratio in Figures 7.4, 7.5 and 7.6 are less than 1.0, so this would appear to suggest that the 55 MHz winds tend to slightly underestimate the 33.2 MHz winds. However, if we are to be consistent with our assumption that both sets of measurements contain equal error ($\sigma_x = \sigma_y$) then this would be reflected in the estimates of g_0; i.e. g_0 should be consistently less than 1.0. Clearly this is not the case as there are cases where g_0 is greater 1.0 while the mean ratio is less than 1.0. The mean ratio estimate is more susceptible to outliers than regression method for determining g_0, so caution must be taken when using it as a metric. Both the zonal and meridional curves in the correlation and mean ratio plots show similar features in that both curves are somewhat parallel with height. The meridional curve shows better results until approximately 95 km where both curves intersect and cross over. Both the mean ratio and correlation coefficient indicate a bias of between 10 to 20% which is minimized typically around a compromised peak height between the two systems at 88 km.

As mentioned previously it is impossible to determine uniquely the values for σ_x, σ_y and g_0 unless more information is known about either of the parameters or we can assume that σ_x=σ_y, thus enabling us to uniquely determine g_0. For the comparison between the two meteor systems we can use this approach based upon the following assumptions.

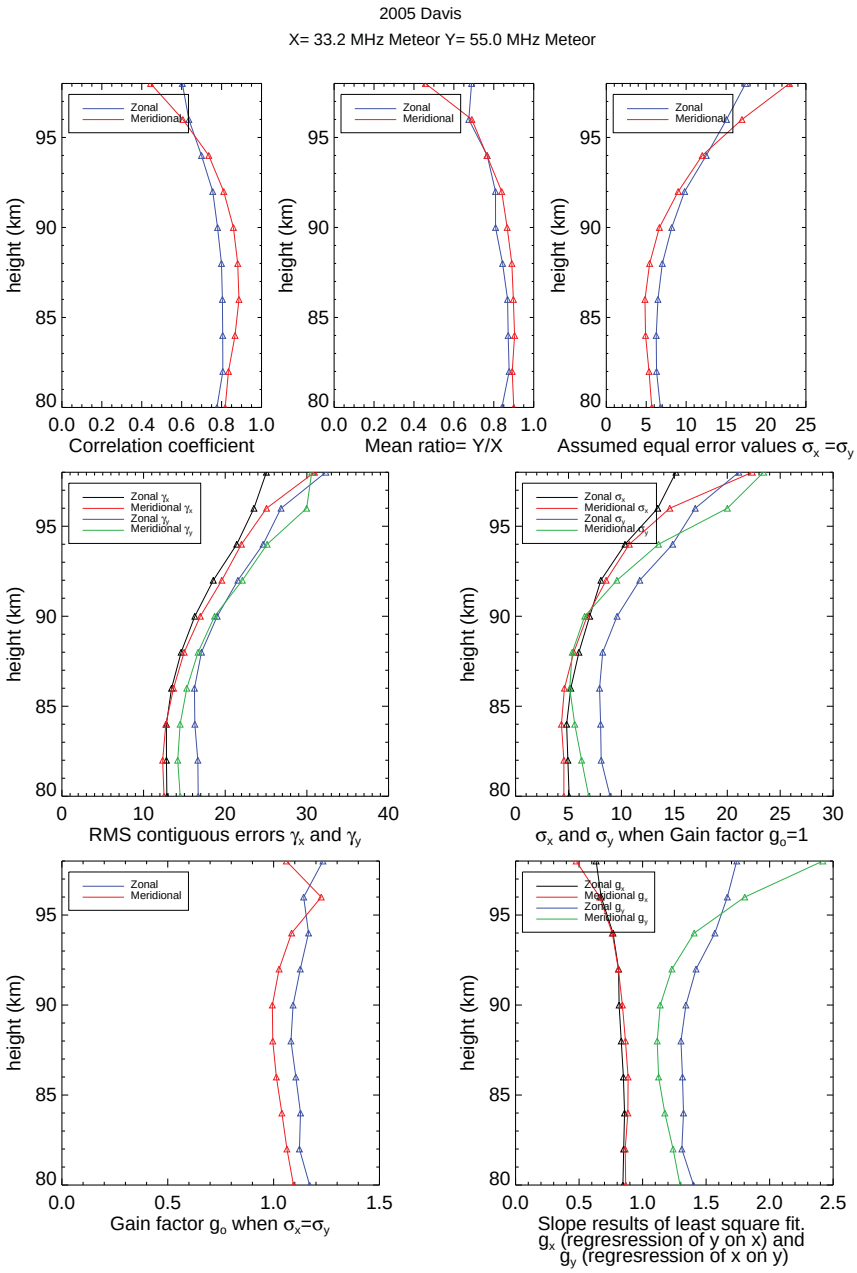

Figure 7.4: The above plots demonstrate the variation in statistical parameters as a function of height for the 2005 Davis 33.2 MHz and 55 MHz meteor radar wind comparisons.

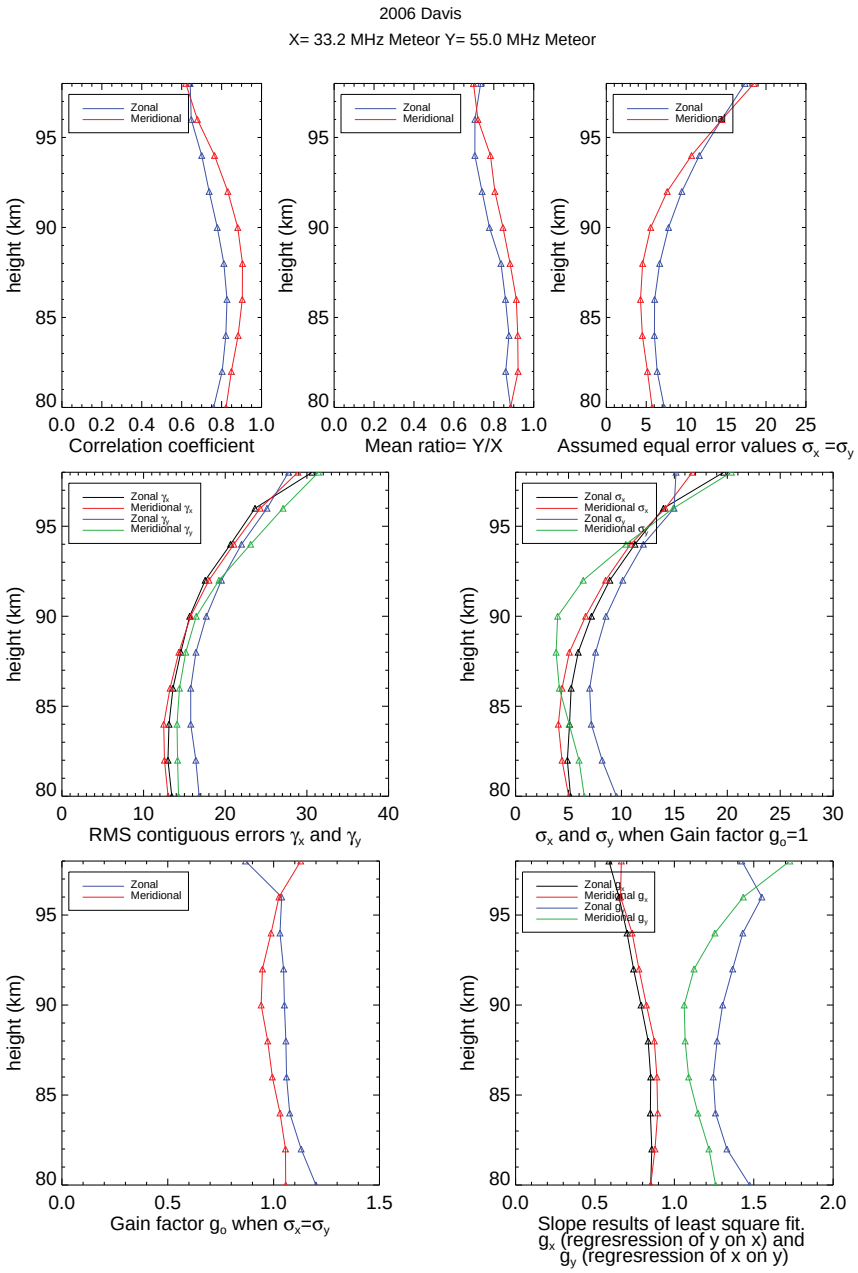

Figure 7.5: The above plots demonstrate the variation in statistical parameters as a function of height for the 2006 Davis 33.2 MHz and 55 MHz meteor radar wind comparisons.

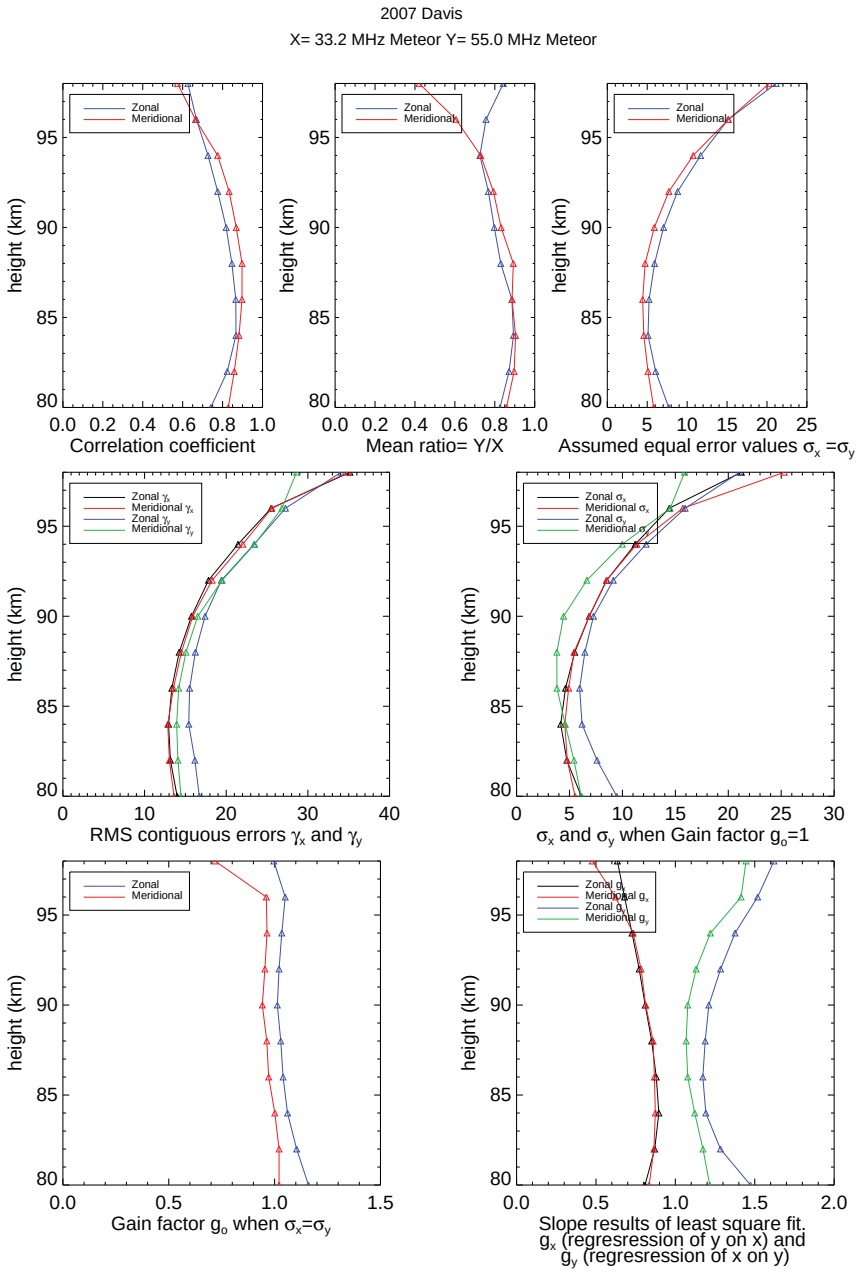

Figure 7.6: The above plots demonstrate the variation in statistical parameters as a function of height for the 2007 Davis 33.2 MHz and 55 MHz meteor radar wind comparisons.

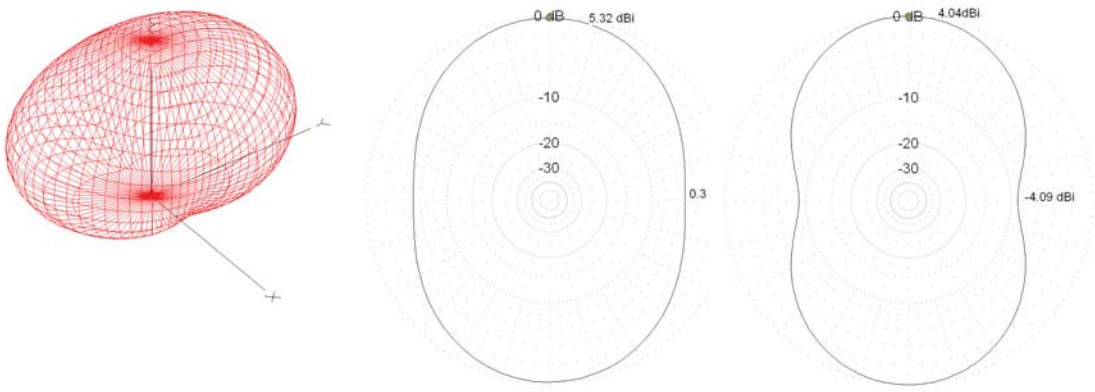

Figure 7.7: The receive antenna polar diagram for the Davis 33.2 MHz and 55 MHz meteor radars. The left diagram depicts the 3D polar diagram. The center diagram shows the antenna gain in the broadside (up page) and endfire (across page) directions at 60° from zenith. The right most diagram shows the antenna gain at 45° from zenith.

- Both systems have been well calibrated for phase error and any other possible system errors.
- The criteria for the minimum number of echoes in order to generate a wind estimate for a particular height time bin is met for both radars.
- Both systems are using the same set of meteors to estimate the wind field over the field-of-view of both radars. While this is not entirely true as can be seen by the daily echo rates (Figures 7.9 and 7.19) we are assuming that the minimum number of echoes criteria to generate a least-squares solution for each time-height bin is met and those echoes used for determining the least-squares solution are the same between both systems.
- Both the 33.2 MHz and 55 MHz signals scatter from different trail diameters and as such the degree of movement of the trail and hence Doppler shift in the return signal is not influenced by the trail diameter.

Looking at the plots for the assumed equal error values in Figures 7.4, 7.5 and 7.6 we can clearly see that the error due to the random noise component is less for the meridional direction compared with the zonal direction. If we

Figure 7.8: 2006 Davis zenith and azimuth count rates. The depression in the distribution of echoes in the zenith plot for the 55 MHz system can be attributed to range aliasing effects which result from running high PRF experiments [Holdsworth et al., 2004].

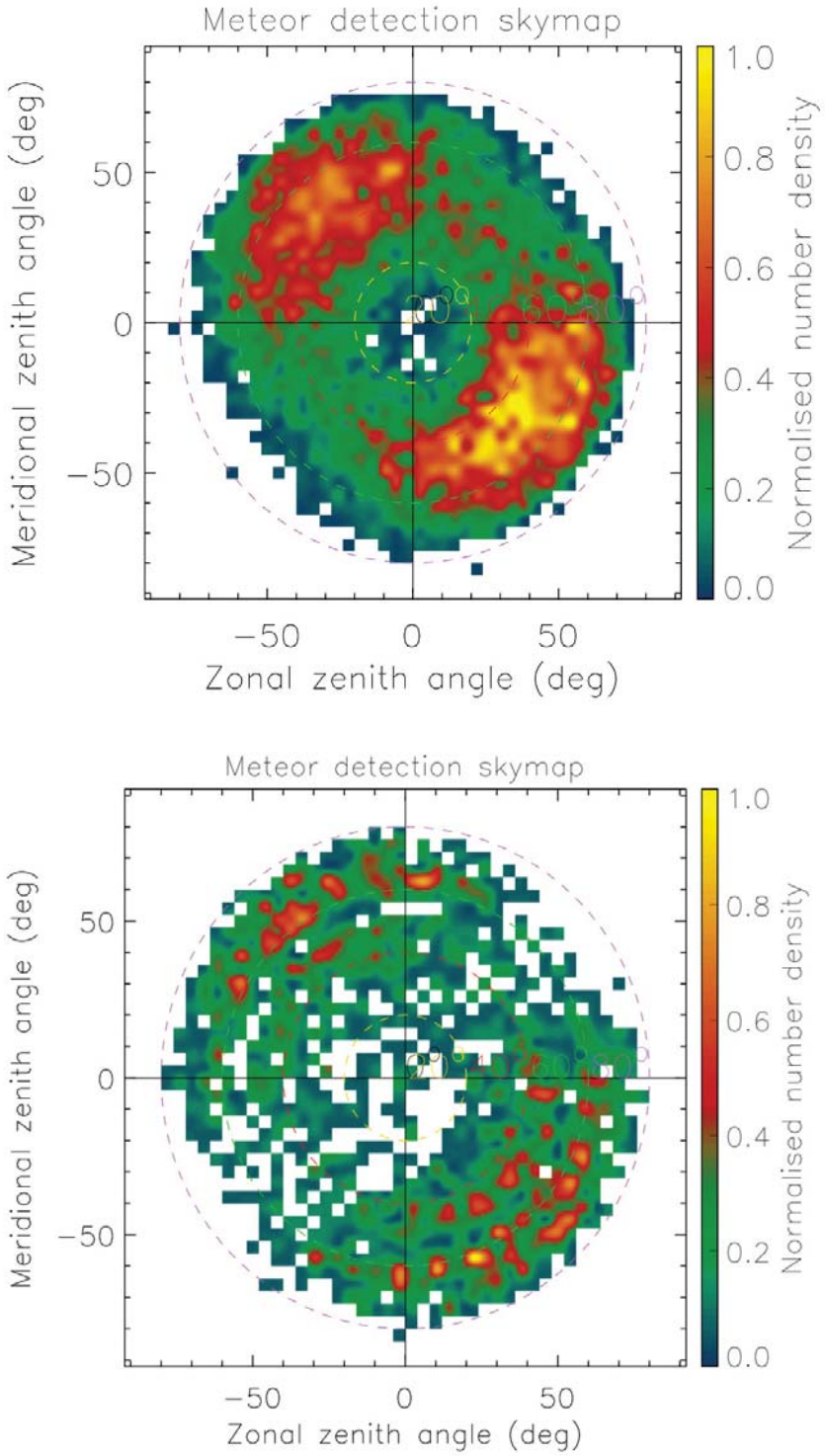

Figure 7.9: The top skymap shows the normalised number density of echoes for the Davis 33.2 MHz system while the botom skymap shows the same but for the 55 MHz system. The concentric circles represent angles of 20°, 40°, 60° and 80° from zenith.

consider 88 km to be a compromise peak height between the two systems such that echo detections are distributed approximately evenly about this height, then one could possibly assume that the shape of the distribution of echo detections could manifest itself in the results. Quite clearly this is not the case as can be seen in the plot for assumed equal error values. The error in the meteor observations increases rapidly above 90 km with the zonal and meridional curves intersecting and crossing over at approximately 95 km as observed with the correlation and mean ratio plots. Similar features are observed in the plots for the RMS contiguous error and σ_x and σ_y for g_o=1.0 plots. This trend could suggest that the variation in the error for both radars is a result of the sampling of wave motions in the atmosphere, rather than solely due to the observed height echo rate distribution.

The RMS contiguous error is a measure of the error between contiguous time points of the data set. The plots for the RMS contiguous error in Figures 7.4, 7.5 and 7.6 show the result for both zonal and meridional components of both systems. The black and red curves correspond to the 33.2 MHz meteor system and the green and blue curves correspond to the 55 MHz system. It is quite clear from the plots that this error is greater for the 55 MHz system than the 33.2 MHz system. This result seems somewhat intuitive when considering that the operation of the 55 MHz system is interleaved with other non-meteor experiments. This means the time interval between detections of meteors and subsequent wind samples used to estimate the wind field is greater than that for the 33.2 MHz system and as such would lead to the larger RMS contiguous error. The larger RMS error associated with the 55 MHz could also be a result of incorrect sampling of gravity waves that can manifest itself as apparent noise within the time series and serve to increase the RMS error of the signal.

Looking at the plot of the gain factor g_0, it is observed that the meridional value is closer to 1.0 and more so in 2007, implying that the assumption σ_x=σ_y is not unreasonable to make despite the zonal component not quite showing as good a result. This enables us to uniquely determine what the error associated with the random noise components δx_i and δy_i for the 33.2 MHz and 55 MHz systems is. It also provides us with a unique window of opportunity when comparing the meteor observations with those of the MF radar (see Section 7.3). The results in Figures 7.4, 7.5 and 7.6 have provided a means of characterising the error associated with the meteor systems which we can apply to the comparison of wind estimates made between the meteor

systems and both the O-mode and X-mode of the MF system. These results can be seen in Figures 7.12 to 7.15 and C.2.

The plots of σ_x and σ_y when g_0=1 in Figures 7.4, 7.5 and 7.6, use the assumption that a 1:1 correspondence between the measurements of the signal component v in both data sets with variance Σ_v^2. This enables us to uniquely determine the error associated with the random noise component of each of the data sets. The results are similar to the results where the assumption of σ_x=σ_y was made. An interesting point to note from this plot is that the error associated with the random noise component of the 55 MHz system (σ_y) decreases below that of the 33.2 MHz system above 86 km in the meridional direction. The RMS contiguous error, which contains both the signal error (Σ_v^2) and noise error (σ_v^2), however shows a gradual increase with height. This suggests that the variance (Σ_y^2) associated with the signal component ($\{v\}$) of the meridional component must increase over this height region in order to maintain the same RMS contiguous error. Looking at both of the plots for the RMS contiguous error and the plot for σ_x and σ_y when g_0=1, where both the zonal and meridional errors are comparable in both plots, this would suggest the signal variance for the 33.2 MHz measurements (Σ_x^2) is somewhat consistent between directions. This however is not the case over the entire height range for the variance Σ_y^2 for the 55 MHz measurements. These results could suggest that there is incorrect sampling of wave motions, i.e. $\{v\}$, which would manifest itself as an increase in the variance Σ_y^2 of the signal $\{v\}$ as observed.

If we consider the final plot in Figures 7.4, 7.5 and 7.6 we can see that the results are quite consistent through the years. Two interesting features in the regression fits of x on y and y on x are present. In the results of the regression of the 55 MHz data on the 33.2 MHz data (black and red curves), there is almost a constant result over the height range, whereas the results from the regression of 33.2 MHz on 55 MHz there is more of an approach to unity at the peak height before diverging, which further suggests that the echo rate at each time-height bin has a significant impact upon the quality of the wind estimates produced by the radars. Given that the zonal and meridional components of the 33.2 MHz system show better agreement than the 55 MHz system, this could imply that there is some form of systematic error associated with 55 MHz system. Looking at the overall results for the 55 MHz system, it would suggest that this error would have to be associated with the zonal component of the system, which would further serve to explain

more of the observed scatter in the zonal measurements scatter plot.

Another means by which to investigate the statistical consistency of wind estimates between two different systems is to look at the statistical distribution of the differences in estimated wind velocity components (e.g. Cervera and Reid [1995], Tsutsumi and Aso [2005], Franke et al. [2005]). If we look at Figure 7.10 we are able to gain insight into how the differences between velocity measurements at a particular height are distributed and also determine the most probable difference between the two measurements. In the plots in Figure 7.10 the green vertical bars indicate one standard deviation (σ) from the mean (μ). The mean of the distribution is indicated by the red dashed line. Once the histogram of the differences is computed for all heights, a Gaussian function is fit to the distribution to estimate the mean μ and variance σ^2 of the histogram distribution assuming that the probability of a particular velocity difference is described by Gaussian statistics; i.e. $\Delta v \sim P_G(\mu, \sigma^2)$. Both the mean and variance for each distribution were determined using the ATRAD "gaussfit.pro" function which is based upon the standard IDL library "gaussfit.pro" routine. In each of the plots in Figure 7.10 we can see that the distribution of differences is larger (i.e. greater standard deviation) for the zonal component than for the meridional component. This is consistent with the observations made with the correlation analyses and scatter plots where the meridional component exhibits higher correlation values (less scatter) than the zonal component.

In order to investigate what is happening over all heights within the height range we have summarised the results of the histogram analysis in Figure 7.11. In the plots of the mean difference in Figure 7.11 it can be seen that the zonal difference increases from 80 km before returning to zero at approxmiately 96 km. The meridional difference remains quite consistent about zero with only minor deviation. The results are quite consistent over the three years 2005, 2006 and 2007, with 2006 showing a slightly more accentuated increase in the zonal difference. Using the result of Hocking and Thayaparan [1997] whereby they concluded that low echo rates produce suspect winds, intuitively an initial reaction would be to expect that the differences between the wind velocity estimates would converge toward zero at the peak height, where the echo rate is maximum, and diverge from zero moving away from the peak height where the echo rate is minimum. As can be seen by the mean differences this is not the case. This would suggest that ambiguities in wind velocity estimates are governed by more than just the

echo rate in a particular time-height bin and that possibly sampling effects or spatial averaging (i.e. what echoes were selected for estimation of the radial velocity component) could contribute to the observed ambiguities. It is interesting to note that both the standard deviation of the zonal and meridional differences shows a similar trend to the RMS contiguous error estimated in the regression analysis as well as the error associated with the random noise component of the measurements. Furthermore, this would appear to suggest that effects other than echo rate, in particular time-height bins, are strong contributing factors when accounting for the observed constant standard deviation until $\sim$90 km before increasing. Now that we have compared the two meteor systems together and have an estimate of the error associated with those systems, in the next section we can apply the result to the comparison of the meteor winds with the co-located MF radar winds, as well as look at how well the meteor and MF winds compare.

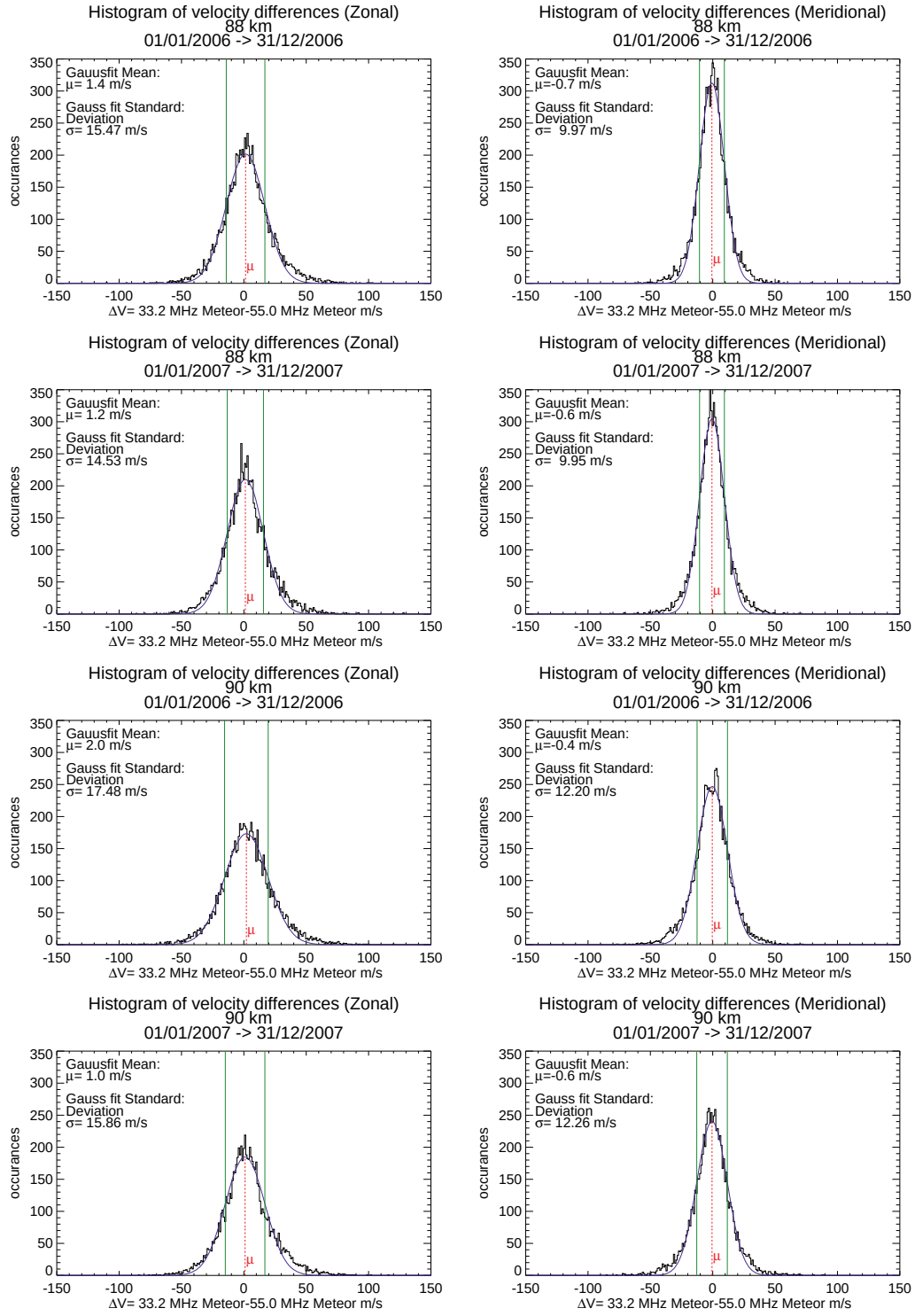

Figure 7.10: The histogram distributions for the differences in zonal and meridional wind velocity estimates at 88 and 90 km for Davis 2006 and 2007.

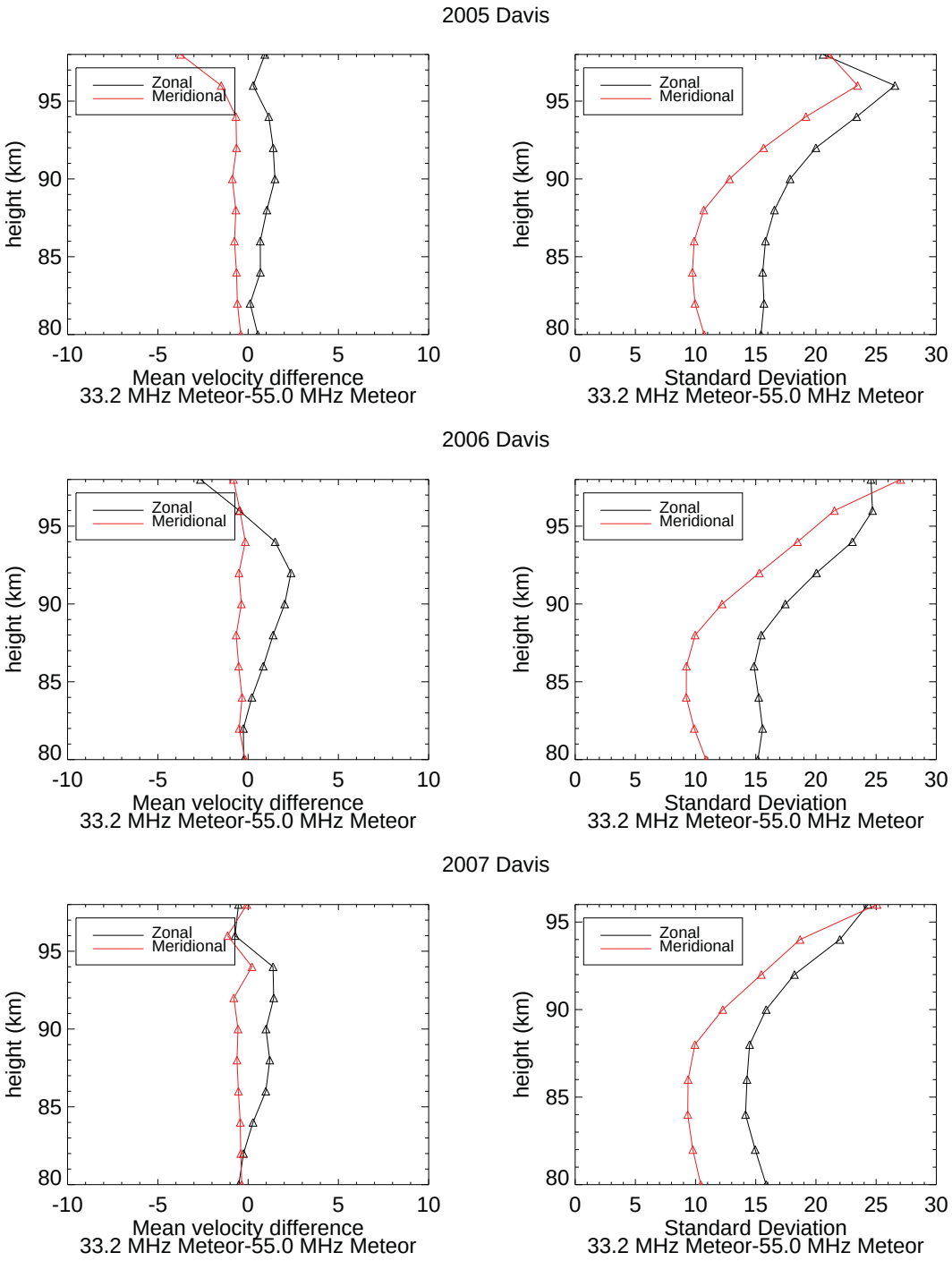

Figure 7.11: Summary of histogram fit results for the 33.2 MHz and 55 MHz meteor comparisons. It is interesting to note that both the gaussfit standard deviations and the error statistics estimated using the regression analysis technique show very similar trends as a function of height.

7.3 Davis MF and Meteor Comparisons

Comparisons between MF and meteor observations have been made on several occasions (e.g. Cervera and Reid [1995], Hocking and Thayaparan [1997], Jones et al. [2003], Tsutsumi and Aso [2005], Kumar et al. [2007]), however comparisons of winds between three co-located independent radar systems is somewhat unique. The comparisons performed by Cervera and Reid [1995] and Hocking and Thayaparan [1997] did not include the full regression analysis as outlined in section 7.1.1. They also only utilised the results of a single regression fit of MF data on meteor data and the comparisons were made upon wind speed and not the components of the wind field as presented in this study. The comparisons performed by Jones et al. [2003], Tsutsumi and Aso [2005], Kumar et al. [2007] employed the regression analysis technique described in section 7.1.1. In these cases there were only two instruments using different techniques and as such there was no justification for the assumption of equal error between the random noise components of the measured signals (σ_x=σ_y). Nor was there any additional information available in order to determine unique solutions for the values of σ_x, σ_y and g_0.

The MF radar at Davis operates alternately in two separate modes of circular polarisation transmission, O-mode and X-mode. The analysis uses Full-Correlation Analysis (FCA) to produce analysed data files for each of these modes. The presence of Earth's magnetic field results in differences in the propagation characteristics of the two polarisations. The X-mode is affected more by absorption and group retardation in an ionised atmosphere in comparison to the O-mode [Ratcliffe, 1975, Tsutsumi and Aso, 2005]. Both modes of operation provide wind estimates over the majority of the height range depending upon time of year and as such the results from both modes can be combined to create an effective measurement. Comparisons of the individual modes with the meteor observations will clearly show that this is not suitable. The MF radar provides approximately two minute wind estimates compared with the meteor radar which provides hourly averaged estimates. This means that in order to compare the two MF data sets with the meteor measurements, hourly averages of the MF winds were required. There are several techniques one can apply to determine an hourly average, however in order to minimise the differences between the two radar techniques, the same hourly averaging process that is applied to the meteor wind analysis was applied to the MF two minute winds in order to determine suitable

hourly averages for comparison. Figures 7.20 and C.3 show the Signal to Noise Ratio (SNR) for the 3 receivers used in the spaced antenna analysis for 2006 and 2007. The SNR can be used as a first order indication of the return signal quality and the likelihood of where the highest quality wind estimates can be found. The height regions in Figures 7.20, C.3, 7.24 and C.6 that are shaded in green indicate an SNR of approximately 35-40 dB above the noise floor of the receivers and as such we have elected to restrict our analysis to this height range (80-98 km). This height region also encompasses the region where the majority of meteor echo detections occur.

7.3.1 Meteor vs. MF O-Mode

Comparisons between the 33.2 MHz meteor and MF O-mode and 55 MHz meteor and MF O-mode are presented herein. Examples of the scatter plots for both comparisons can be found in Figures 7.12 and 7.13. The scatter plots illustrate the results of the regression of MF O-mode data on the meteor data (red line) and the meteor data on the MF O-mode data (blue line). The green line is the gain factor g_0 when the equal error assumption has been made. At this point it is not clear that that this assumption is appropriate, the result has been included for completeness along with providing an indication of the quality of that particular assumption in this case. The final piece of information is the purple line in Figures 7.12 and 7.13. As mentioned previously, in previous studies there were no grounds upon which one of the three statistical variables, σ_x, σ_y or g_0 could be eliminated allowing an analytical solution of the remaining two unknown parameters to be found. The purple line represents this unique analytical result which has been made possible by having three co-located independent systems. From the previous comparison of the two meteor systems whereby the assumption of σ_x=σ_y was made, an "average" value for $\sigma_x = \sigma_y = \sigma$ was determined over the height range 80-90 km where the error was considered to relatively constant to a first order approximation. Subsequently g_0 was determined from the substitution of the average value of σ into the regression equations in section 7.1.1 used in the comparison of the MF O-mode and meteor data. This result is plotted as the purple line. While the "average" error over the height range does not provide a 100% statistically sound basis for determining the error in the meteor technique over the height range, it was considered to be to a first order approximation and a unique means of eliminating one of the unknown

variables in the MF O-mode meteor comparisons. An interesting result to note is that the slope of the purple line in most cases is quite close to that of the green line in Figures 7.12 and 7.13. This would appear to suggest that the assumption of equal error between the meteor and MF O-mode observations may in fact be a plausible assumption to make in most cases in order to estimate errors and g_0 to first order.

Given the similarity between the results of 2006 and 2007, only the 2006 results are presented in this chapter for discussion. The results for the 2007 comparisons can be found in Appendix C. The results from the scatter plots over the height range for comparison of both meteor and MF O-mode winds are summarised in Figures 7.14 and 7.15. Both the meteor and MF O-mode exhibit good correlations over the height range; typically 0.7-0.8 for 2006 and 0.7-0.9 for 2007. Unlike the comparison between the two meteor systems where there was a consistent difference over the height range between the zonal and meridional results, there is better agreement between directions in the comparisons with MF O-mode and meteor data. Both zonal and meridional components show similar correlation values from 86-98 km in 2006 and 88-90 km in 2007. The mean ratio of the wind components show a gradual decline from 82 km in both 2006 and 2007 for the 33.2 MHz MF O-mode comparison but less so with the 55 MHz MF O-mode comparison. It is generally accepted that the MF FCA technique produces underestimates of the wind speed which can be attributed to "Triangle-size effect", undersampling of the diffraction pattern due to small pattern scale and relatively large pattern velocities and saturation of receivers [Golley and Rossiter, 1970, Cervera and Reid, 1995, Holdsworth and Reid, 1995, Hocking and Thayaparan, 1997, Holdsworth and Reid, 2004a,b, Tsutsumi and Aso, 2005]. Looking at the regression results, there is a bias of between 20 to 30% which is minimized at approximately 86 km which is close to the peak height of the meteor echo distribution and generally accepted to be the best return height for the MF system. Cervera and Reid [1995] indicate that meteor echo detections ($\sim$10% of all detections) from side-lobes or low elevation (large zenith) angles can lead to overestimates in the meteor winds by as much as 20%. Since the two meteor systems are all-sky systems, low elevation angle detections will still have an effect on wind estimates. The ATRAD analysis software does not have an option for limiting the zenith angle range of echoes used in wind velocity estimates, however more recent analysis techniques of meteor wind velocity estimates serve to prevent or minimise introduced biases through a

quality control of echoes used in the wind estimates. See Section 2.4 and Holdsworth et al. [2004]. In previous MF and meteor comparisons [Hocking and Thayaparan, 1997, Tsutsumi and Aso, 2005] it was observed that underestimates in the MF FCA winds became prevalent at heights $\geq$ 90 km. From the results of the mean ratio of the winds and the estimation of g_0 in the MF O-mode to 33.2 MHz meteor comparison, there is a constant decrease in mean ratio and g_0 starting at 82 km. On the other hand the results in the 55 MHz and MF O-mode comparison exhibit more constant values between 82 and 90 km with a more rapid decrease in these quantities above 90 km. This result is more consistent with what has been observed by Hocking and Thayaparan [1997], Tsutsumi and Aso [2005]. This would appear to suggest that the 33.2 MHz meteor winds are overestimated. Given the result of the verification of McKinley's echo rate formula, the lower frequency of operation increases the number of echoes detected which one could argue would also increase the number of echoes detected at low elevation angles which contribute to the overestimation of meteor winds.

As a first order means of determining the reliability of wind estimates for both systems, the meteor height echo distribution and the MF SNR as functions of height offer an good indication. If we consider the MF O-mode SNR plot in Figure 7.20, we can see that the SNR is consistently around the 35-40 dB level over the 80 to 98 km height range while the echo rate (see Figure 7.19) exponentially increases below and peaks sharply on or about 90 km followed by an exponential decrease. Given the more constant SNR with height of the MF O-mode, it would be reasonable to assume that the quality of the wind estimates would be more consistent over the 80-98 km height range. The results in Figures 7.14 and 7.15 clearly show more consistency between the zonal and meridional components between both systems. The 55MHz and MF O-mode comparison exhibits slightly more consistency between directions compared with the 33.2 MHz and MF O-mode comparison. This would indicate that either the 55 MHz and the MF O-mode winds contain a bias, less so with the MF O-mode winds, or the 33.2 MHz winds contain bias or quite possibly there could be a bias associated with all three systems. An interesting result can be seen in the plots for σ_x and σ_y for when g_0=1. In 2006 from 88 km and then in 2007 from 92 km, the error in the meridional component drops to zero. In this case, the scatter plot indicates that the slope relating both measured data values drops well below 1.0 and as such the result from the regression of x on y is greater than 1.0 means upon

inversion, the value for $g_y < 1.0$. This implies g_0=1 would in fact not be a valid solution. The values for g_y in these cases are typically within 0.3 % of 1.0 and as such in the interest of maintaining a bounded solution for (7.22) we have used g_0=1.0 as a further bounding solution and set $g_y = 1.0$ in these cases. This results in σ_y=0 as observed in the plot of σ_x and σ_y for g_0=1.0 in Figures 7.14 and C.1. Initially it was thought that this could be a floating point precision issue as IDL's default floating point representation format is only 32-bit single-precision. This was ruled out when the calculations were repeated using IDL's 64-bit double precision floating point representation as the same results were obtained. It is believed that the real problem lays in the surd relationship between σ_x, σ_y and g_0 and the computer's inability to solve surd relations with 100% accuracy. This result is also consistent with the notion that the 33.2 MHz winds are in fact overestimated. Coupled with the known biases present with MF SA winds which are underestimated this would lead to such a strong skewing of the scatter that subsequently would result in an estimate for $g_y < 1.0$.

The techniques of both the meteor systems and the MF system are different as they ustilise different methods of determining the components of the wind vector and both have different fields of view. The field-of-view for the meteor systems Tx polar diagram as can be seen in Figure 4.3 which is more akin to an omni-directional radiator. The Davis MF Tx polar diagram is more directional as can be seen in Figure 3.17. This means that the wind estimates produced by the meteor and MF systems represent two different horizontal spatial averages. An interesting result however can be seen in Figure 7.12. From this it would seem that on or about the peak height, we can make the assumption that both data sets $\{x\}$ and $\{y\}$ contain equal random noise error in both meteor MF O-mode comparisons. This can be seen by the stronger agreement between the green and purple lines in Figure 7.12. This agreement is more evident between the 55 MHz meteor and MF O-mode comparison than with the corresponding 33.2 MHz meteor and MF-O-mode comparison. This could further suggest a common bias between the 55 MHz and MF O-mode which is consistent with observations of slightly better agreement with zonal and meridional components of the statistical quantities from the scatter analysis of the 55 MHz meteor and MF O-mode compared with the 33.2 MHz and MF O-mode comparison. Kumar et al. [2007] found in the comparison between a 35.25 MHz meteor radar and MF radar at Thumba (8.5°N, 77°E) that below 90 km the MF radar appeared

to underestimate the wind by approximately 12% and increases to approximately 78% above 90 km. The results for g_0 in Figure 7.14 would appear to somewhat concur with those found by Kumar et al. [2007]. There is a noticeable decrease in the value for g_0 above 90 km however it is not as severe as in the case of the 33.2 MHz meteor MF-O-mode comparison.

The next stage of the analysis was to perform a histogram analysis between the 33.2 MHz meteor and MF O-mode and 55 MHz meteor and MF O-mode data. Tsutsumi and Aso [2005] performed a similar comparison between meteor and MF derived wind estimates at Syowa, Antarctica (69°S, 39°E), where the meteor winds were derived using the same MF radar operating in meteor mode. Tsutsumi and Aso [2005] increased the height bin size to 4 km and bi-hourly time bins. This was performed in order to increase the number of samples and increase the statistical accuracy of the comparison. In the comparisons made in Figures 7.17 and 7.18, there are enough data points such that a 2 km height bin and 1 hour time bin could be maintained without compromising the statistical accuracy of the result due a lack of data points. The mean difference between the meteor and MF O-mode winds in Figures 7.17 and 7.18 are quite small and comparable with those found by Tsutsumi and Aso [2005]. The results of the of the standard deviation of the differences found by Tsutsumi and Aso [2005] are slightly larger than those found in Figures 7.17 and 7.18, however this could simply be due to the sample size used by Tsutsumi and Aso [2005]. Cervera and Reid [1995] performed a similar comparison between 55MHz meteor and MF radar at BP albeit with a smaller data set. The results for the mean difference and standard deviation at each height bin are also comparable to those shown in Figures 7.17 and 7.18. The results in Figures 7.17 and 7.18 indicate that despite the statistical quantities themselves being slightly less in the case of the 33.2 MHz and MF O-mode comparison, there is slightly more consistency over the height range with the 55 MHz MF O-mode histogram comparisons. This is in agreement with what can be observed in the results of Cervera and Reid [1995] and Tsutsumi and Aso [2005]. Both meteor comparisons with the MF O-mode data show relatively good agreement, however the difference between the MF and meteor results increase significantly above 90 km. This result is consistent with previous comparisons. In the next section we compare the meteor winds with the MF X-mode winds.

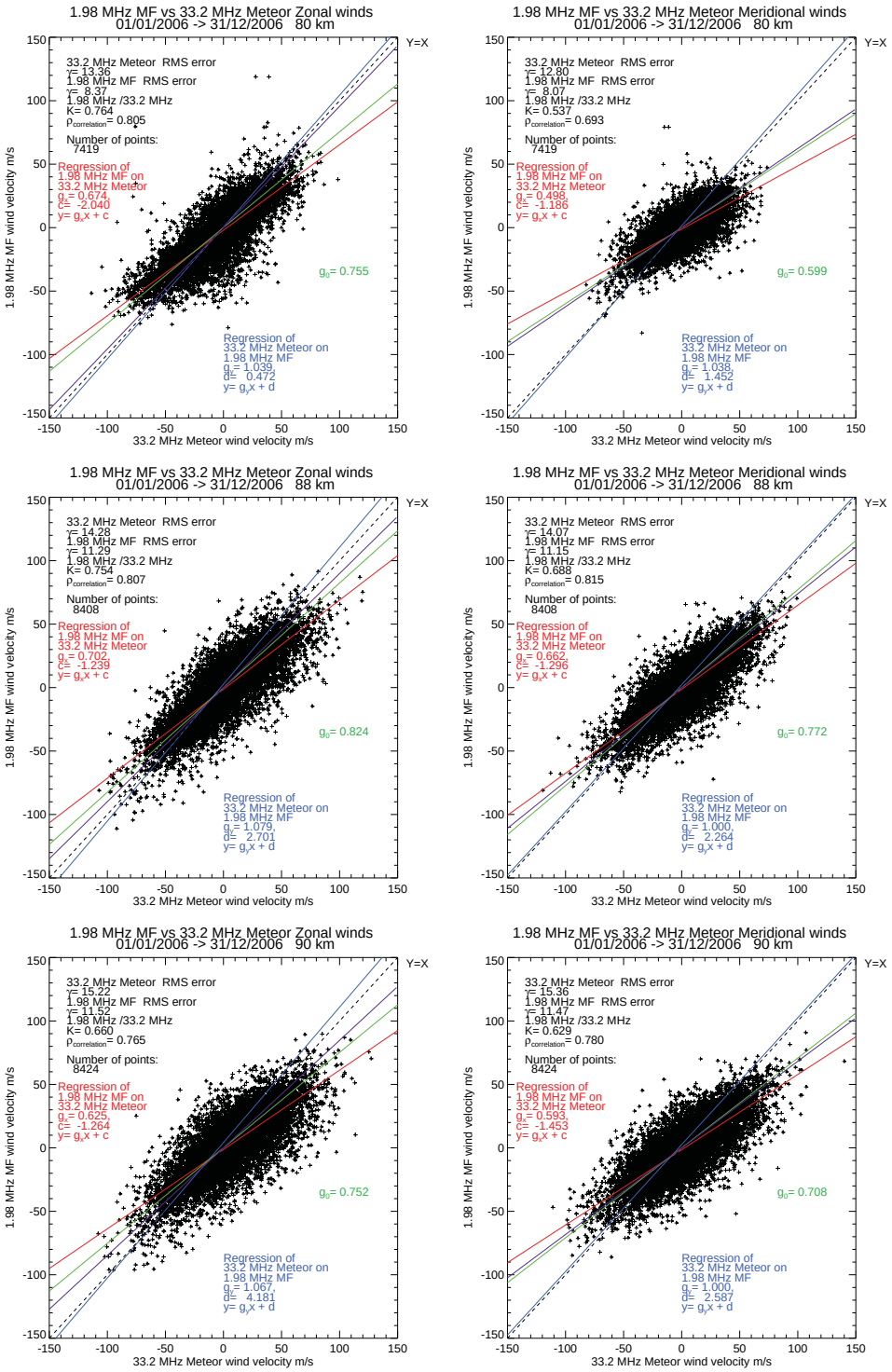

Figure 7.12: Davis MF O-mode and 33.2 MHz meteor scatter plot. The purple line represents the slope derived using the error values from the meteor-meteor comparison when equal error between both meteor measurements was assumed.

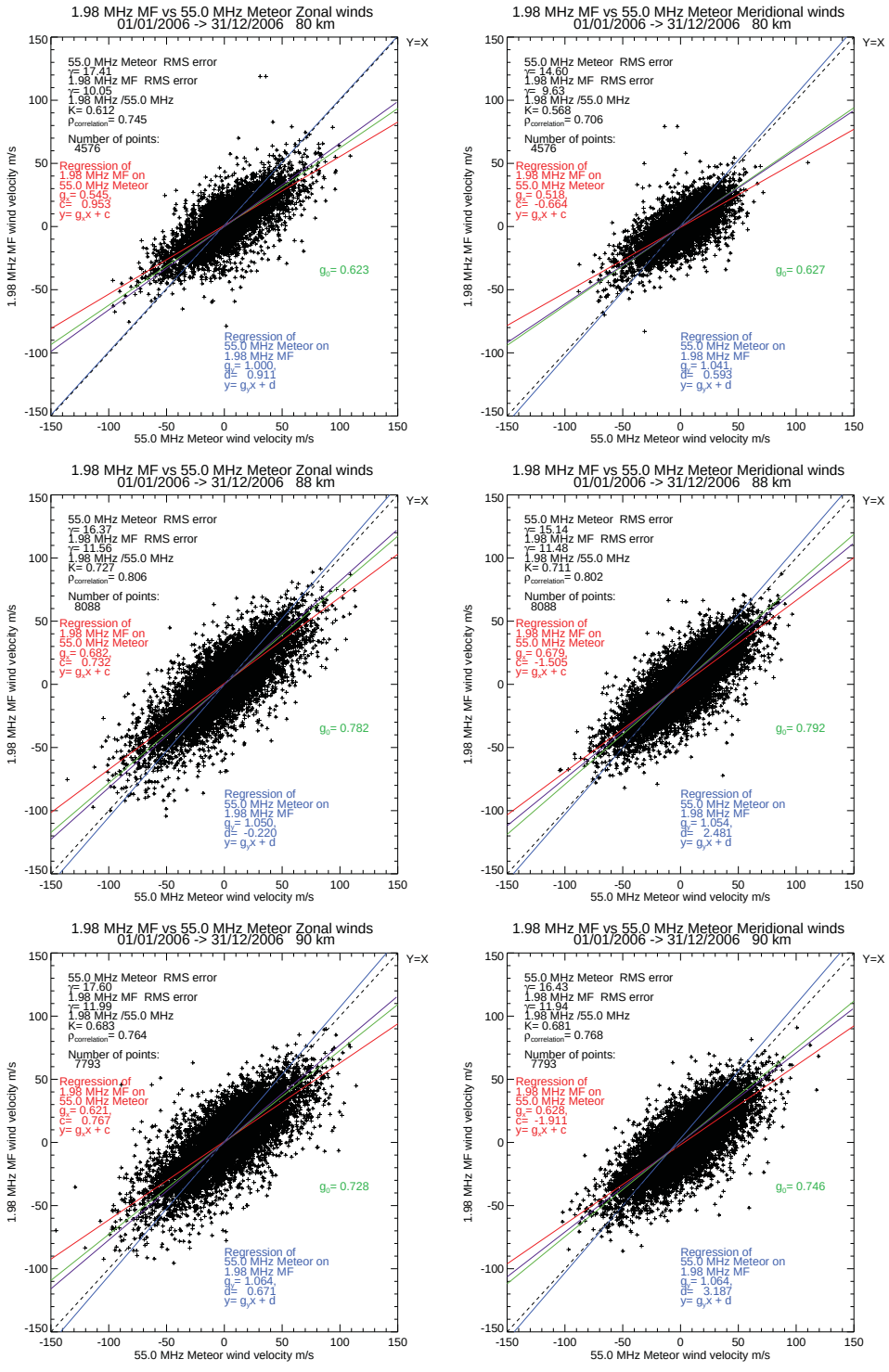

Figure 7.13: Davis MF O-mode and 55 MHz meteor scatter plot. The purple line represents the slope derived using the error values from the meteor-meteor comparison when equal error between both meteor measurements was assumed.

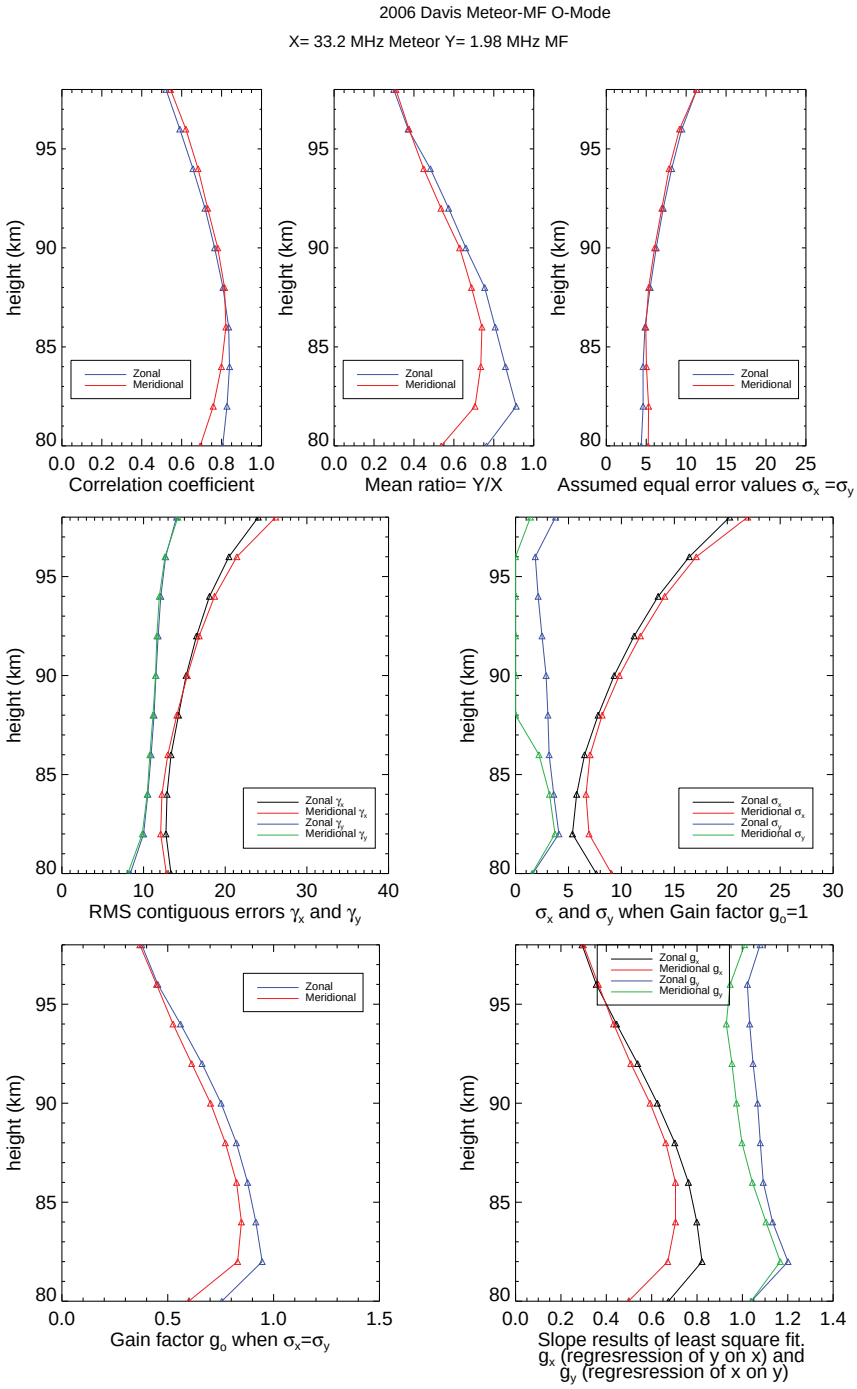

Figure 7.14: Davis MF O-mode and 33.2 MHz meteor scatter plot comparison results. The plots above summarise the results from applying the regression analysis to the data at all heights.

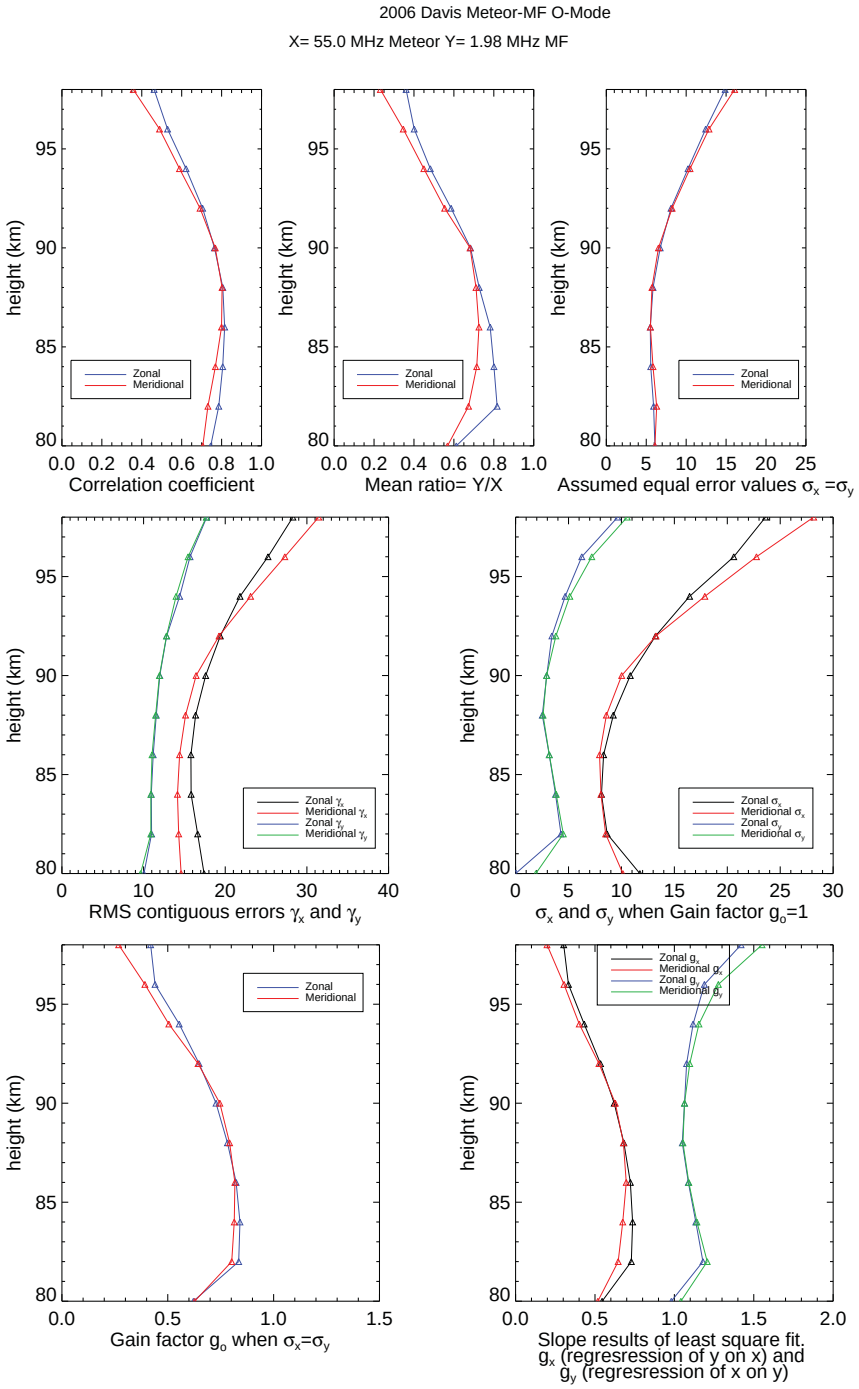

Figure 7.15: Davis MF O-mode and 55 MHz meteor scatter plot comparison results. The plots above summarise the results from applying the regression analysis to the data at all heights.

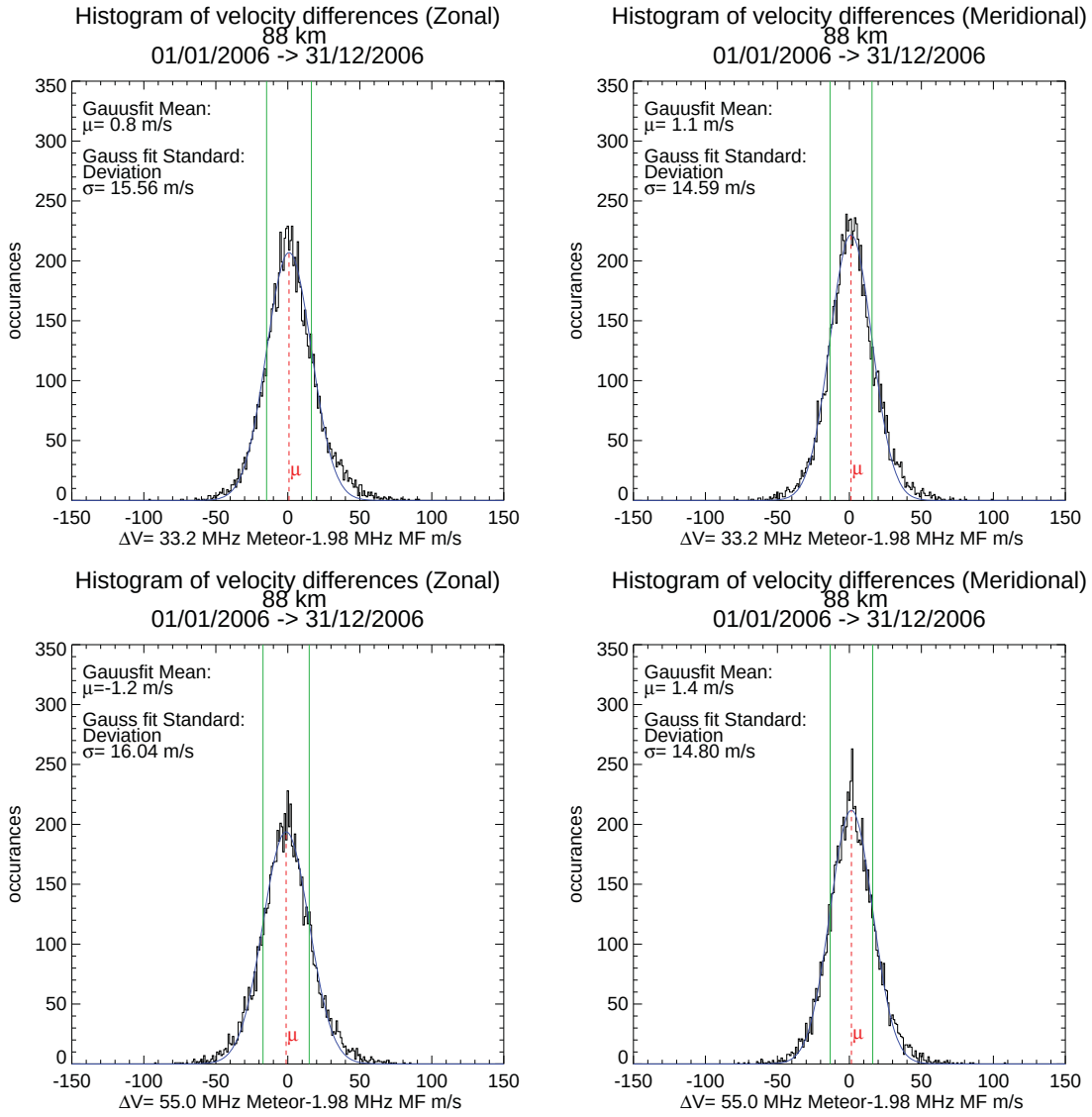

Figure 7.16: Davis 33.2 MHz meteor and MF O-mode and 55 MHz meteor and MF O-mode histograms of velocity differences. The green lines indicate 1 standard deviation and the red dashed line indicates the mean difference.

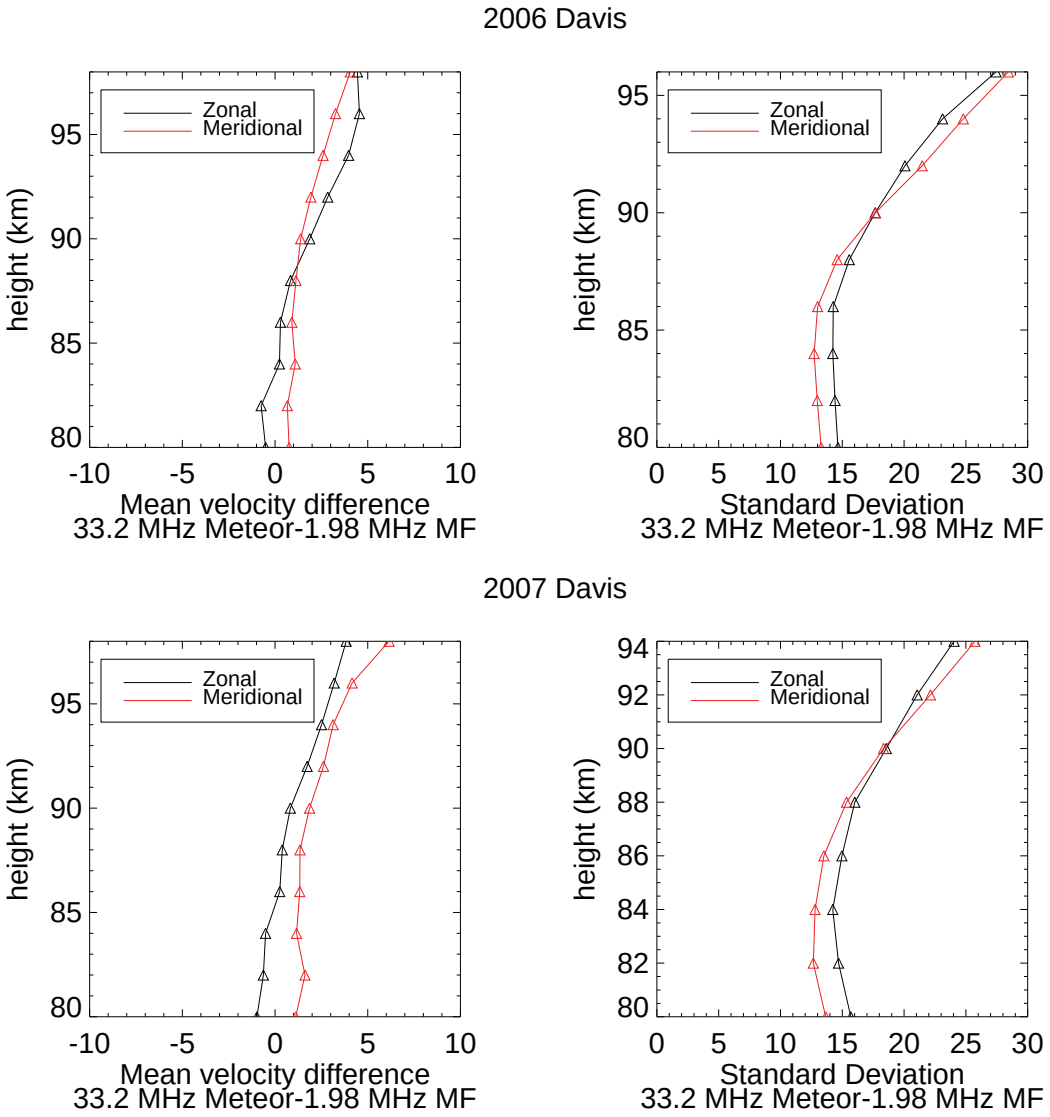

Figure 7.17: Davis 33.2 MHz meteor and MF O-mode summary of histogram velocity differences for 2006 and 2007.

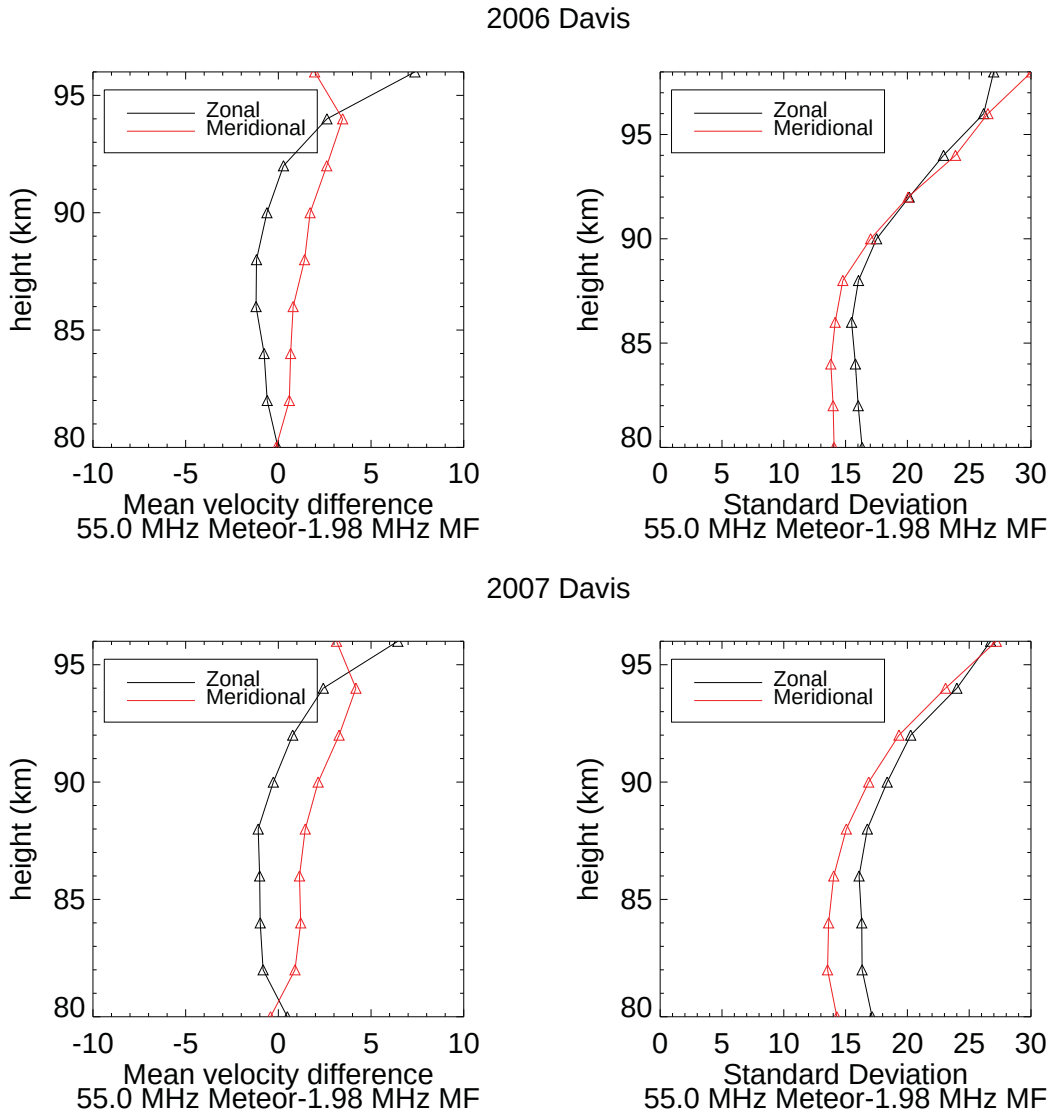

Figure 7.18: Davis 55 MHz meteor and MF O-mode summary of histogram velocity differences for 2006 and 2007.

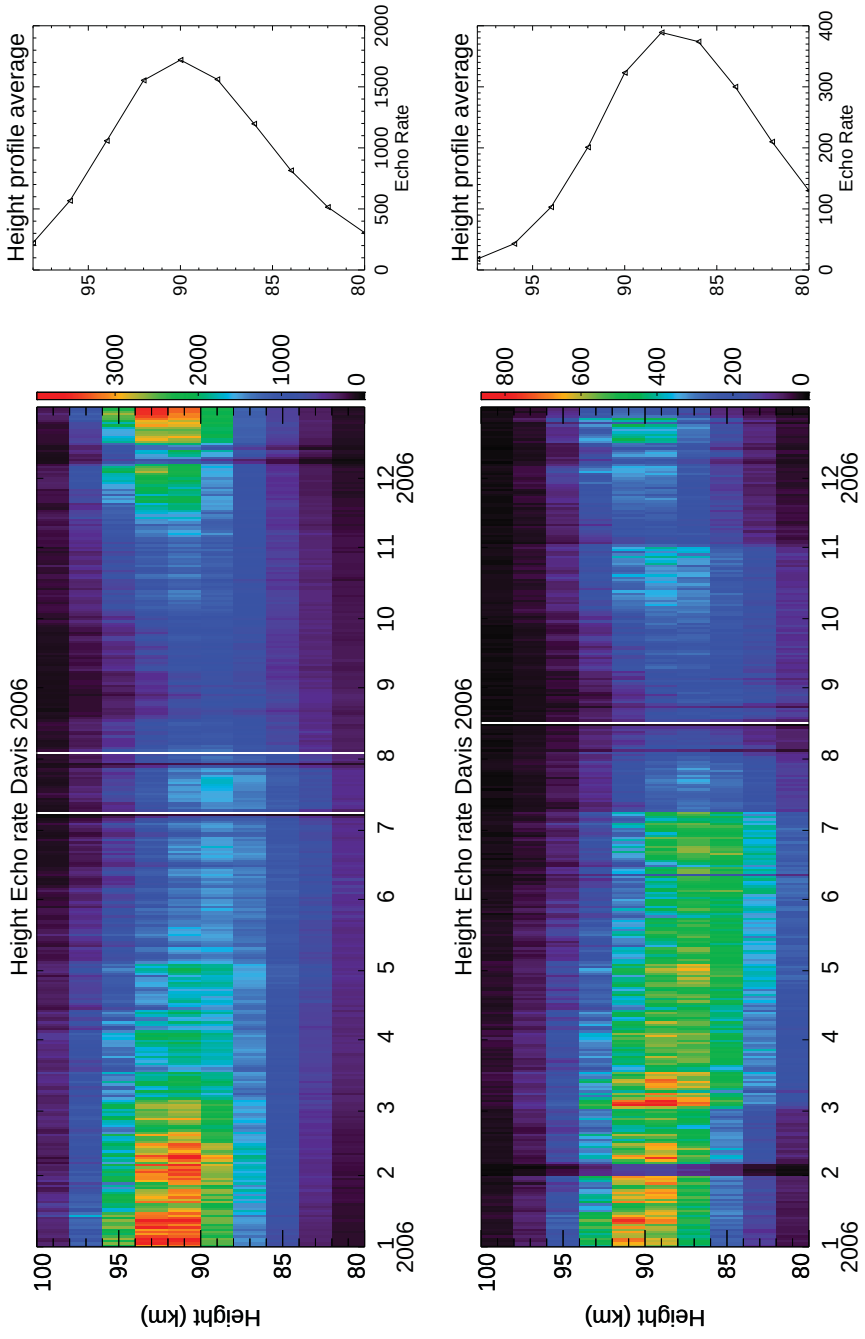

Figure 7.19: 2006 Davis 33.2 MHz and 55 MHz Meteor radar detections. The top row plots are the results for the 33.2 MHz system and the bottom row of plots are the results for the 55 MHz system. The line plots represent the mean echo rate for the period in the image plot for each height. The mean value was determined using an outlier rejection criteria of 2.5 standard deviations.

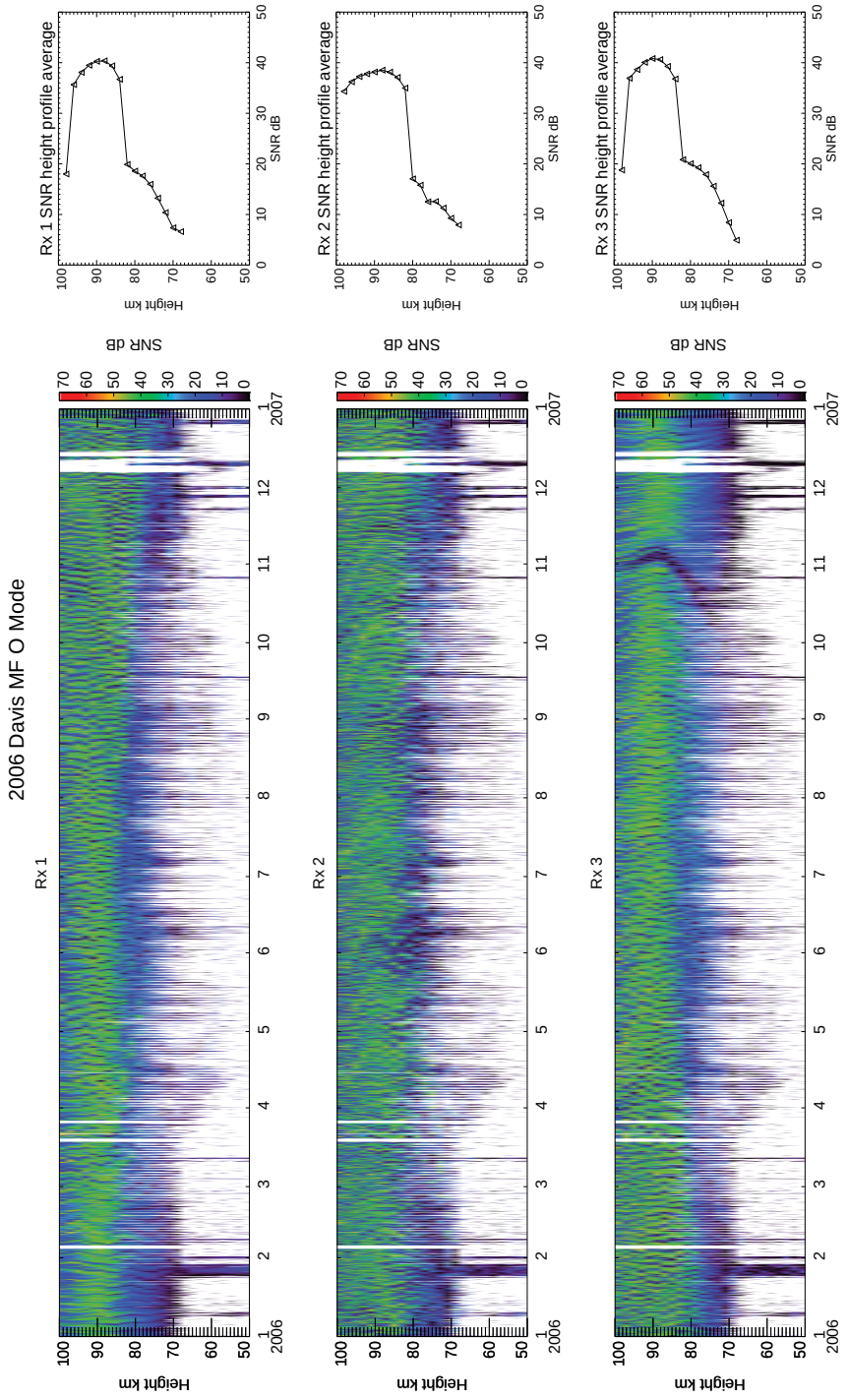

Figure 7.20: 2006 Davis MF O-mode SNR. The line plots represent an effective average SNR profile for each receiver. The inverse log of each point was taken and the mean for each height bin calculated using an outlier rejection scheme with 2.5 standard deviations and the log of the result taken.

7.3.2 Meteor vs. MF X-Mode

Comparisons between meteor and MF winds are now continued with meteor winds and MF X-mode winds. Using the same process used in the previous sections, scatter plots and histograms of the X-Mode winds (Y) and meteor winds (X) were produced and the statistical results are subsequently summarised in Figures 7.21 and C.4 for the 33.2 MHz MF X-mode comparison and Figures 7.22 and C.5 for the 55 MHz MF X-mode comparison. As per the previous comparison, the results from 2006 and 2007 are quite similar and as such only the results from 2006 are presented within this chapter. We can clearly see that in both the 33.2 MHz and 55 MHz comparisons with the MF X-mode, that the statistical quanties at 80 km are quite comparable with those in the comparisons between the meteor and MF O-mode. They do however indicate a clear almost linear decrease in correlation and mean ratio and linear increase in the σ_x and σ_y parameters which strongly suggests that the X-mode derived winds are not suitable for comparisons with the meteor wind estimates above 80 km. This is consitent with the observations made by Tsutsumi and Aso [2005] where the Earth's magnetic field yield different propagation characteristics between the X-mode and O-mode polarisations. The X-mode suffers from more absorbtion and group retardation than the O-mode Mode and as such O-mode winds are chiefly used for comparisons. Comparisons of the MF O-mode with X-mode show very similar similar results to the comparison of the meteor with the MF X-mode (see Figures 7.23 and C.7). This result is not surprising given the agreement between the meteor and MF O-mode winds. This indicates that both the X and O-mode winds should never be combined above 80 km as this would only serve to contaminate the quality of the O-mode wind estimates above this height. Of particular note is the results of the MF SNR plots. The O-mode SNR plots in Figures 7.20 and C.3 show more consistency between the three receivers compared with the X-mode SNR plots in Figures 7.24 and C.6. This may also serve to explain the lack in quality of wind estimates from X-mode operations. The fact that the SNR differs significantly between the three receivers for the X-mode observations could possibly have an adverse affect upon the FCA technique applied to the data from each of the receivers. In the next section we investigate the results of improving the echo rate with the BP 55 MHz meteor system and how well the winds compare to those obtained by the square-kilometre array MF system.

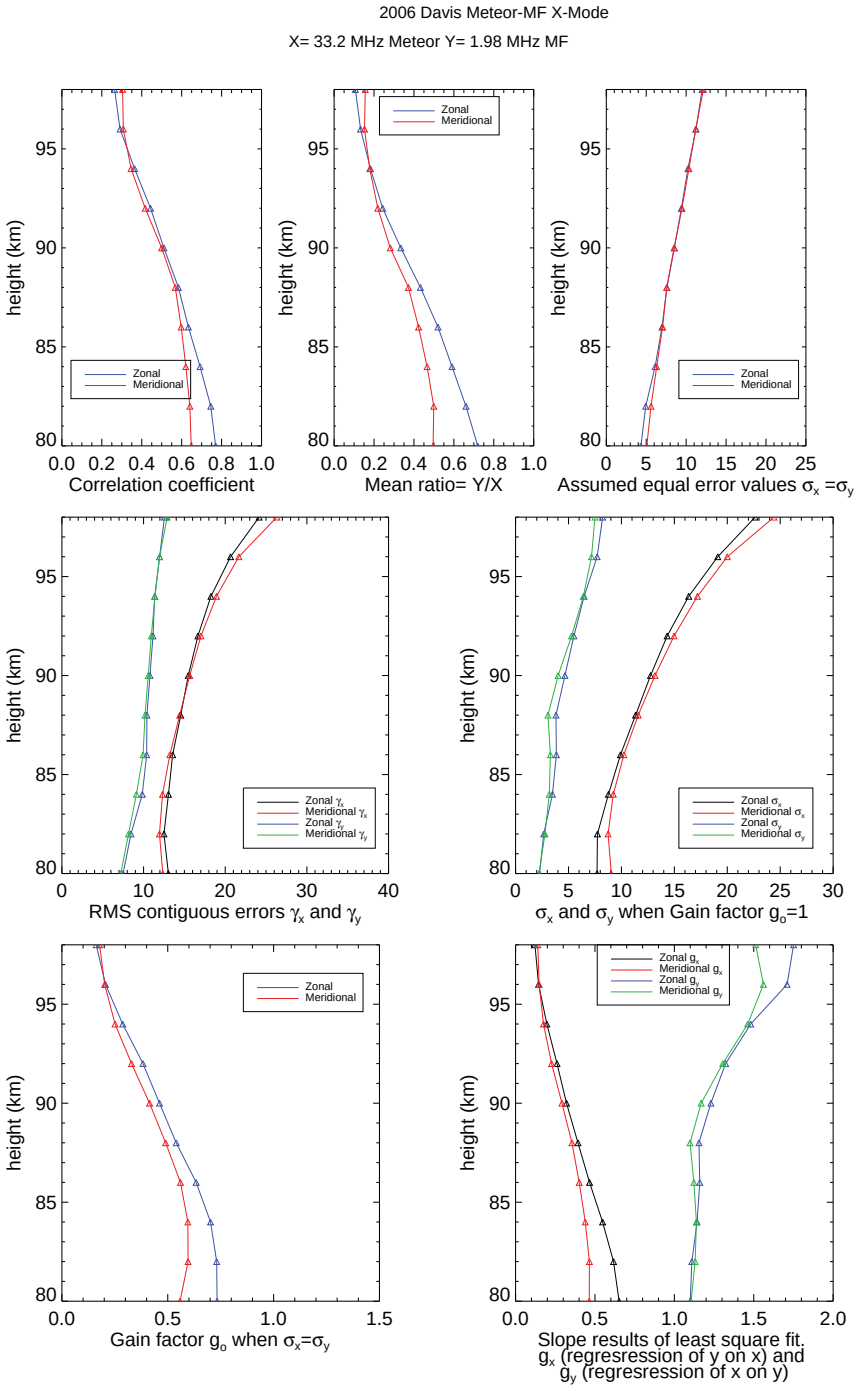

Figure 7.21: Davis 33.2 MHz and X-mode scatter plot comparison summary. Results for 2007 can be found in Appendix C.

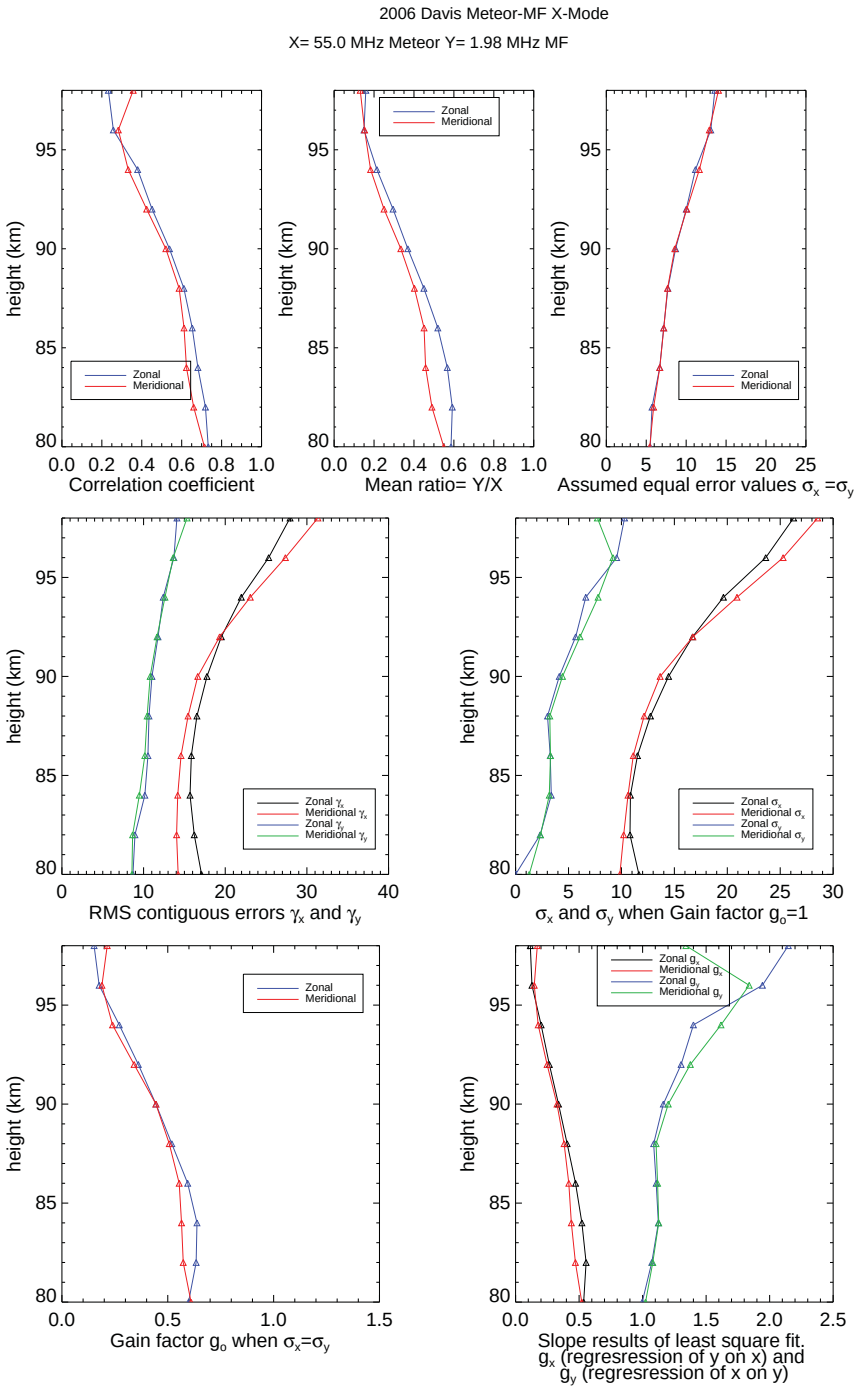

Figure 7.22: Davis 55 MHz and X-mode scatter plot comparison summary.

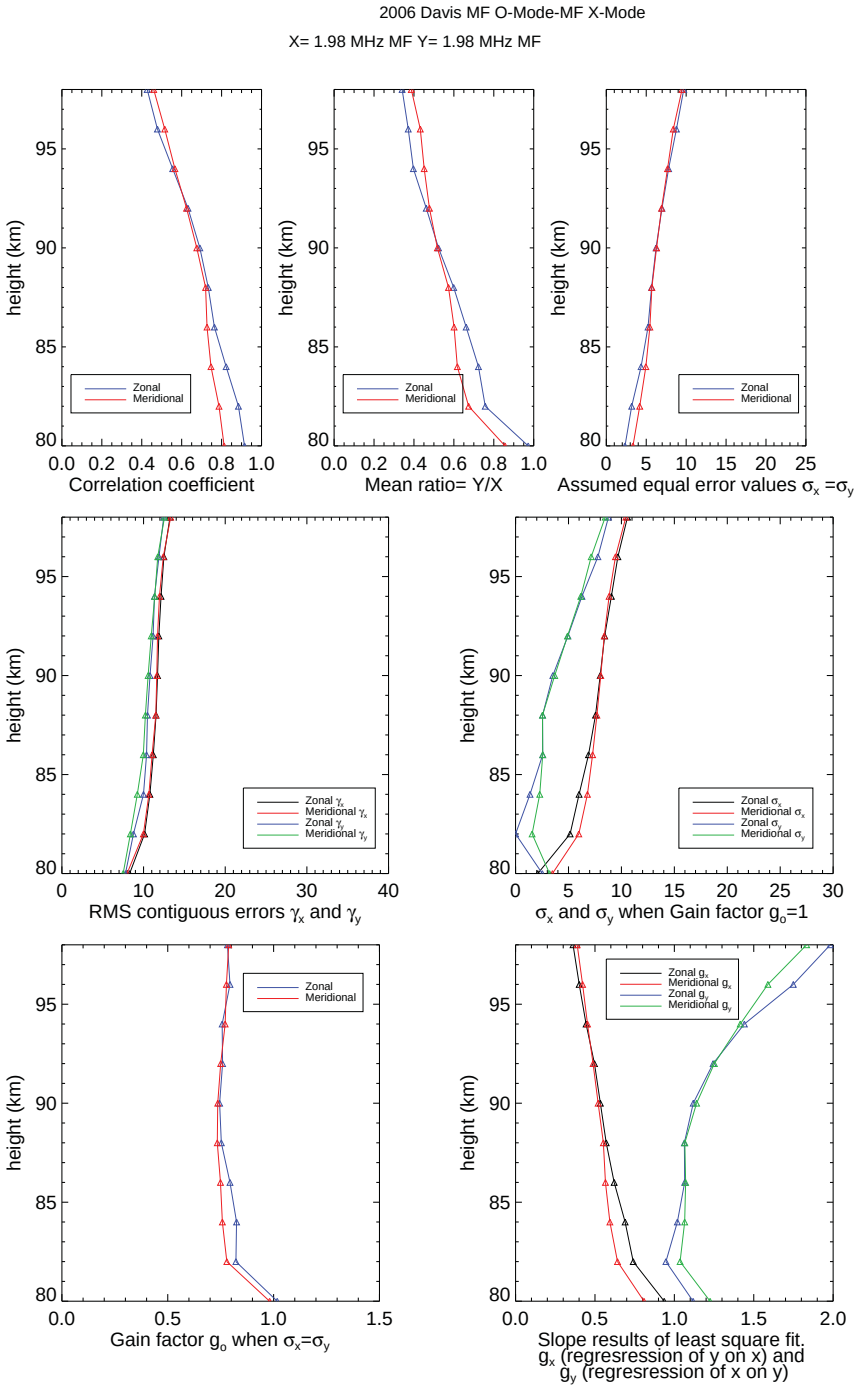

Figure 7.23: Davis MF O-mode and X-mode scatter plot comparison summary.

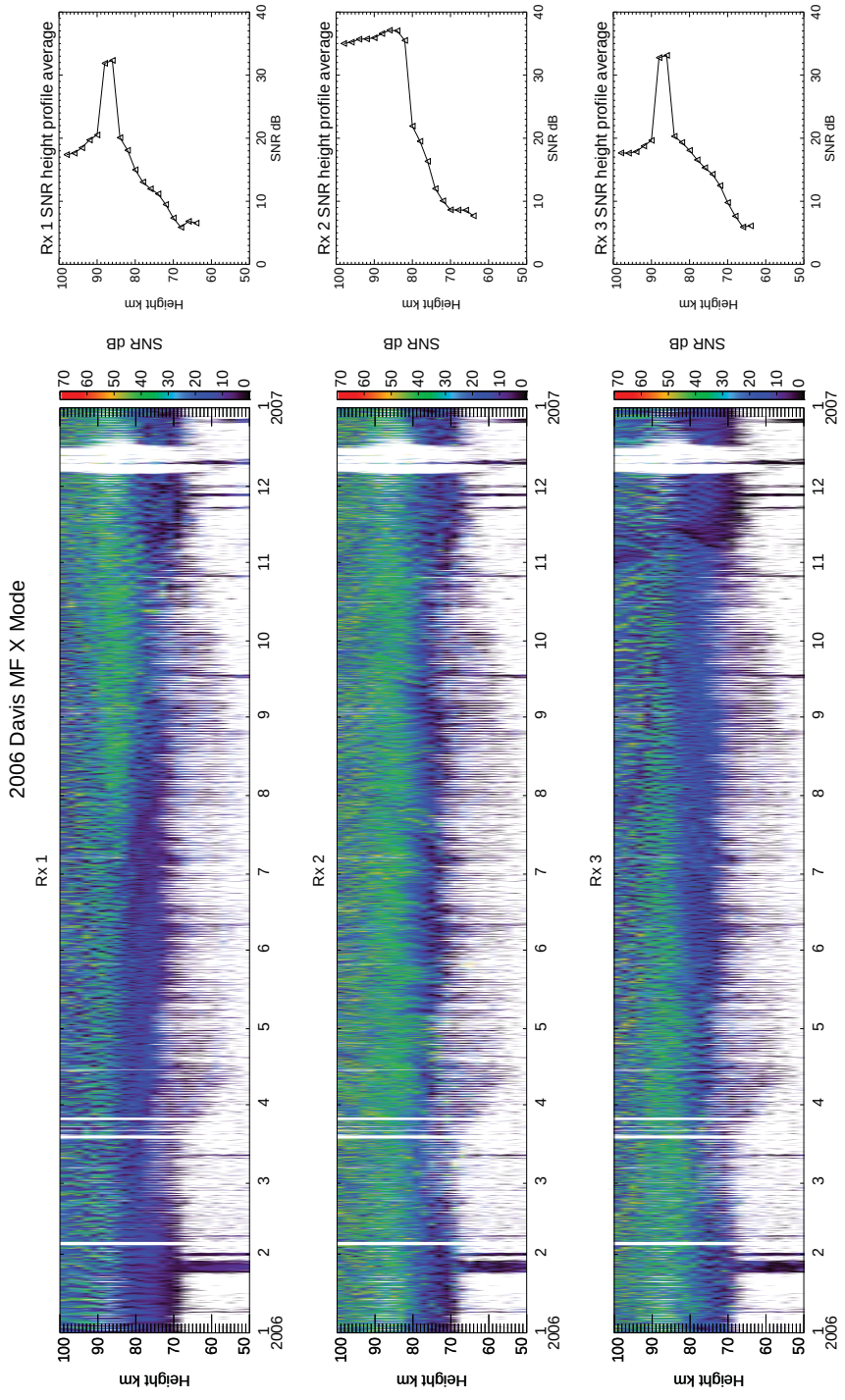

Figure 7.24: 2006 Davis MF X-mode SNR. There is a noticeable discrepancy for the X-Mode in the average SNR profile for receiver channels 1 and 3 between 2006 and 2007 that would indicate a system fault occurred. This would also serve to explain some of the observed differences in the results from the comparisons between the two years.

7.4 Buckland Park 55 MHz Meteor and MF Radar Comparisons

Wind estimates from the BP 55 MHz meteor radar were compared with those of the co-located square kilometre array MF radar. In 2006 the meteor radar was operated using a single VTX PA module (peak power $\sim$ 18 kW, 4% duty cycle) with a brief period where a prototype STX II (peak power $\sim$ 20 kW, 10% duty cycle) transmitter was used (see Figure 7.25). In 2007, the radar was operated by combining all six PA modules from the VTX transmitter (peak power $\sim$ 83 kW, 4% duty cycle after final tuning). Unlike the Davis 55 MHz meteor system, the BP system was operated in dedicated meteor mode. The combination of this mode of operation and the higher transmit power level resulted in a higher observed echo rate in each hour-height bin over the observation period such that it should result in a minimization of the statistical error of wind estimates due to low echo rates for the majority of the height distribution. Unlike the interleaved operation of the Davis 55 MHz system between meteor and ST modes, the dedicated meteor mode of operation would also serve to minimise any potential issues related to the sampling of gravity waves, which should result in a smaller observed signal variance. Despite several cases of downtime of the radar, which included a mouse destroying the data acquisition card, damage to a diode stack in the VTX power supply rectifier circuit, the damage of the antenna balun through water leakage into the 7/16 connector and the damage to the first generation 1:2 splitter-combiner, the data used for the statistical comparison was only from when the radar was performing at its maximum capability. The points utilised in the comparison of the two data sets were those in which both contained valid 'simultaneous' estimates[1]. Once the BP MF data was converted from local time (+9.5 UTC) to UTC it was subsequently hourly averaged using the same technique applied to the Davis MF data. The BP MF radar was operated using two different analysis techniques, Imaging Doppler Interferometry (IDI) and Full Correlation Analysis (FCA). Detailed descriptions of the operation of the BP MF radar in both IDI and FCA modes can be found in Holdsworth and Reid [2004a] and Holdsworth and Reid [2004b].

[1]Valid simultaneous estimates are data points with zero error flag and binned into a common time bin.

The correlation results from the meteor and MF FCA comparison in 2006 are quite similar to the 2007 results showing slightly higher correlation results in the upper heights in 2007 . In 2007, the VTX transmitter was tuned to its optimal performance capability which meant that maximum power was being produced and as such the echo rate was improved. This could account for the slightly higher correlation and mean ratio results. The RMS contiguous error measurements are in close agreement to that of the Davis meteor MF comparisons and tend to be more constant over the height range, even more so in 2007 when the radar was producing more power. This would further suggest, along with the Davis comparison, that the echo rate, particularly in the extremities of the height distribution, plays an important role in the statistical reliability of determining wind estimates. While we cannot strictly say that both techniques contain the same random noise error over the 80-98 km height range, it would appear that this is in fact a fair approximation to make at a height of approximately 86-90 km. 86 km is close to the peak height of the meteor distribution and also represents the best return height for the MF radar. The significance of this is reflected in correlation and mean ratio plot, where these quantities are maximised, and in the plots for σ_x and σ_y where these values are at or close to their minimum value. These results and the results in Figure 7.30 are in fact in strong agreement with the results of Cervera and Reid [1995] where it was found that the strongest agreement between MF and meteor wind velocity estimates occur at 86 km. In 2006 the values for g_0 when we assume equal error are close to 1.0 but fall to less than 1.0 with increasing height. In 2007, these values increase slightly. Given that $g_0 < 1.0$ for the majority of the height range, particularly in the 88-90 km height range where the meteor technique produces its strongest results, this indicates that the MF FCA wind estimates are underestimated which is consistent with the observations of Cervera and Reid [1995], Holdsworth and Reid [2004b] and Holdsworth and Reid [2004a]. Looking at the plots for the mean ratio and g_0 for 2006 and 2007, it would appear that the MF wind estimates are between 10-20% less than the meteor winds at 86 km.

The plot of the regression results in Figures 7.28 and 7.29 along with the results from the histogram analysis in Figure 7.30 indicate that there is better overall agreement between wind estimates from both radars in the meridional direction compared with the zonal direction. Similar results can be found in Tsutsumi and Aso [2005], Hall et al. [2005]. The characteristic of better agreement with the meridional component compared with the zonal

component appears to be common with the southern hemisphere comparisons presented in this study. Cervera and Reid [1995] do not present results for both zonal and meridional components of the wind, however it is clear from Figure 7 in Cervera and Reid [1995] that there are in fact some large discrepancies between the MF FCA and meteor zonal measurements. It is important to note that the meteor radar used by Cervera and Reid [1995] was a narrow beam radar which utilised beam steering techniques as opposed to the all-sky interferometric meteor system used in this comparison. The narrow beam width in combination with beam steering techniques result in a smaller field of view compared with the all-sky system. These differences which effectively result in different horizontal spatial averages between the two systems are enough to possibly account for discrepancies between this comparison and that of Cervera and Reid [1995]. The beam was also only steered in the zonal direction. The comparison found in Kumar et al. [2007] does show better agreement in the zonal results than the meridional results which is agreement with the findings of Hall et al. [2005]. The comparison in Kumar et al. [2007] was performed on observations made in the Northern hemisphere where as this comparison and that of Tsutsumi and Aso [2005] were performed on observations made in the Southern hemisphere. The difference could be attributed to the Equatorial Electro Jet or one could possibly appeal to a dynamical argument to explain this discrepancy.

By investigating the plots of meteor, MF FCA and MF IDI superposed winds in Figure 7.35, there a couple of observations that can be made in regards to the wave characteristics. It can be seen that there is in fact a variation in both the phase difference between the meteor and MF results as well as an increase in the wave amplitude with height measured by the meteor system. The variation in phase difference is an indication of vertical wave propagation and as such one would expect the wave amplitudes to increase with height as observed by the meteor radar [Tsutsumi and Aso, 2005]. The results from this study, albeit over a smaller height range exhibit the same characteristics as those observed by Tsutsumi and Aso [2005]. At heights above 90 km, it can be seen that the amplitude of the semi-diurnal component increases with height in the meteor wind observations, but exhibit less variation with the MF observations. Although a more extensive height range is required by this study to fully compare with the results of Tsutsumi and Aso [2005] and Hall et al. [2005], from the results available there is agreement with these findings. Tsutsumi and Aso [2005] have hy-

pothesized that the MF winds from the lower heights (less than 90 km) are contaminating the winds in the upper heights, however there is no clear explanation available as to how or why this is occuring. In order to properly investigate the observations of varying phase lag between MF and meteor observations as well as the variation in tidal amplitude, a harmonic analysis is required. The results from the statistical comparisons performed between the MF and meteor observations strongly support the observations of the increasing difference between MF and meteor winds.

Considering the results of the histogram of velocity differences analysis, it can be seen that the mean difference between the two data sets significantly changes between 2006 and 2007. The standard deviation of the distribution of velocity differences, however, appears to remain the same. Consider the plots of meteor AOA in Figure 7.27. The zenith angle plots are almost identical between 2006 and 2007. The azimuth plots show a significant difference in 2007 in that there is a second distinguishable peak at approximately 270°. There is a second peak present in the 2006 azimuth count plot, however it is not a prevalent as in the 2007 plot. This could help explain why the mean difference between MF and meteor winds in 2007 in the zonal direction is closer to zero compared with 2006 over the the height range.

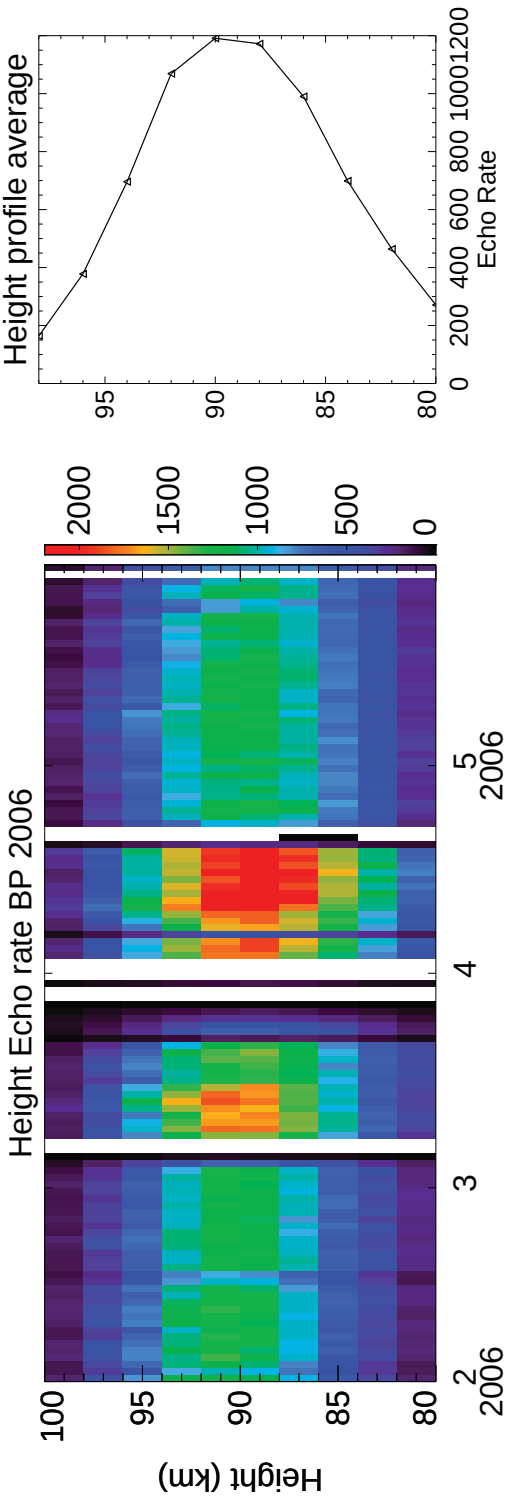

Figure 7.25: 2006 BP 55 MHz meteor radar meteor detections. The burst of counts in the middle of April is when the STX II prototype was trialed at BP. The meteor experiment on the STX II had duty cycle of $\sim 8\%$ giving an average power of ~ 1.6 kW, which is greater than the single PA VTX configuration that gave and average power $\sim$ 700 W.

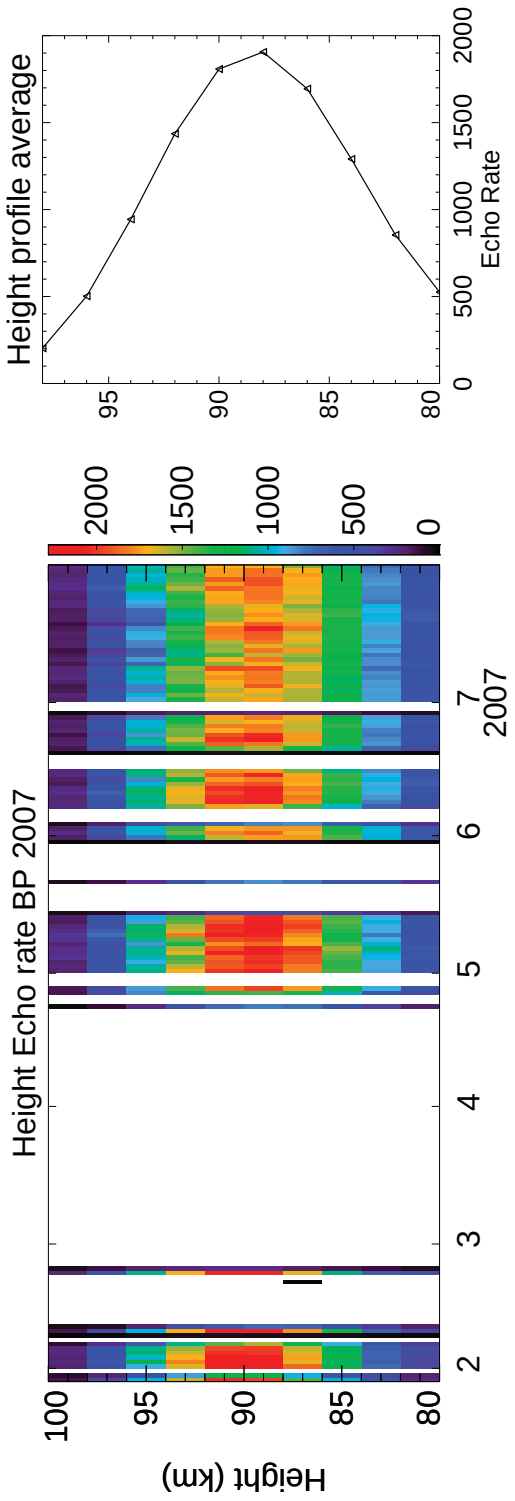

Figure 7.26: 2007 BP 55 MHz meteor radar meteor detections. The radar was operated utilising all 6 PA modules. The meteor experiment on the VTX had a duty cycle of $\sim 3\%$ giving it an average transmit power of ~ 2.1 kW.

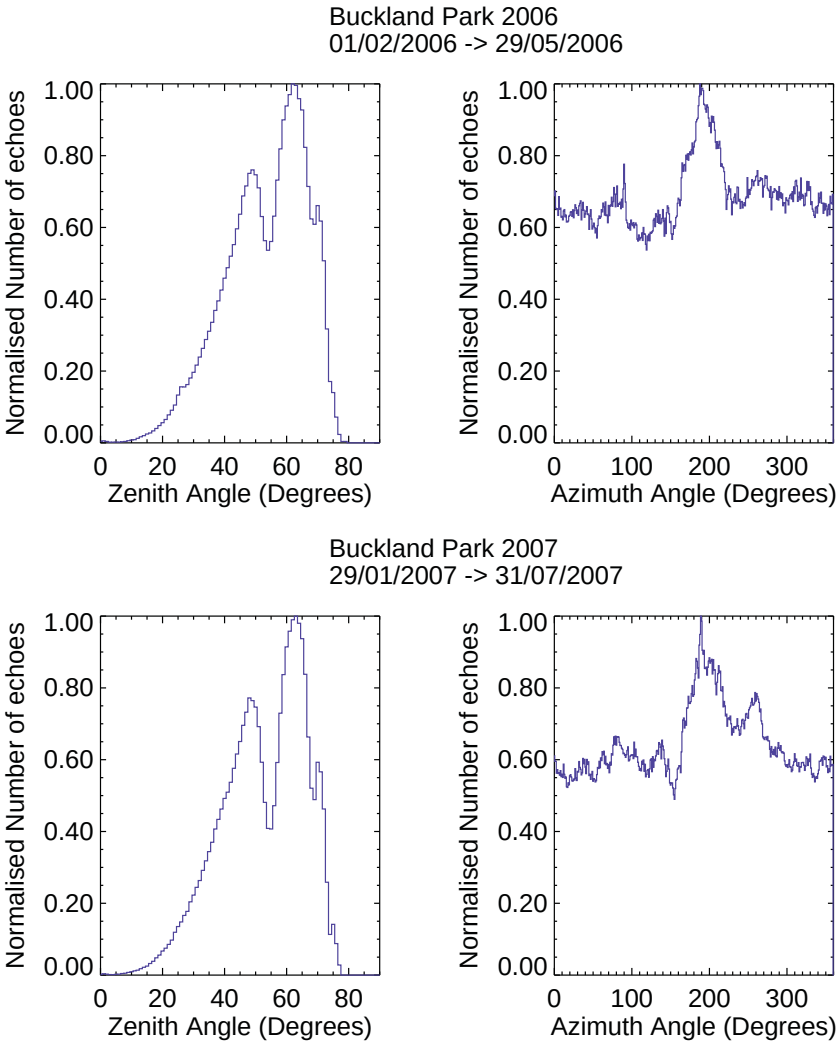

Figure 7.27: 2006 and 2007 BP 55 MHz meteor zenith and azimuth counts. We can see from the azimuth plots that we don't get the same dip in count rate with azimuth angle as we did with the Davis meteor systems. This is due to the use of crossed dipole receive antennas on the BP system and the resulting polar diagram which is more isotropic. The dips in count rate with zenith angle are the result of running high PRF experiments which results in range aliasing effects (see Holdsworth et al. [2004]). The second peak in the 2007 azimuth plot could possibly be the result of shower activity.

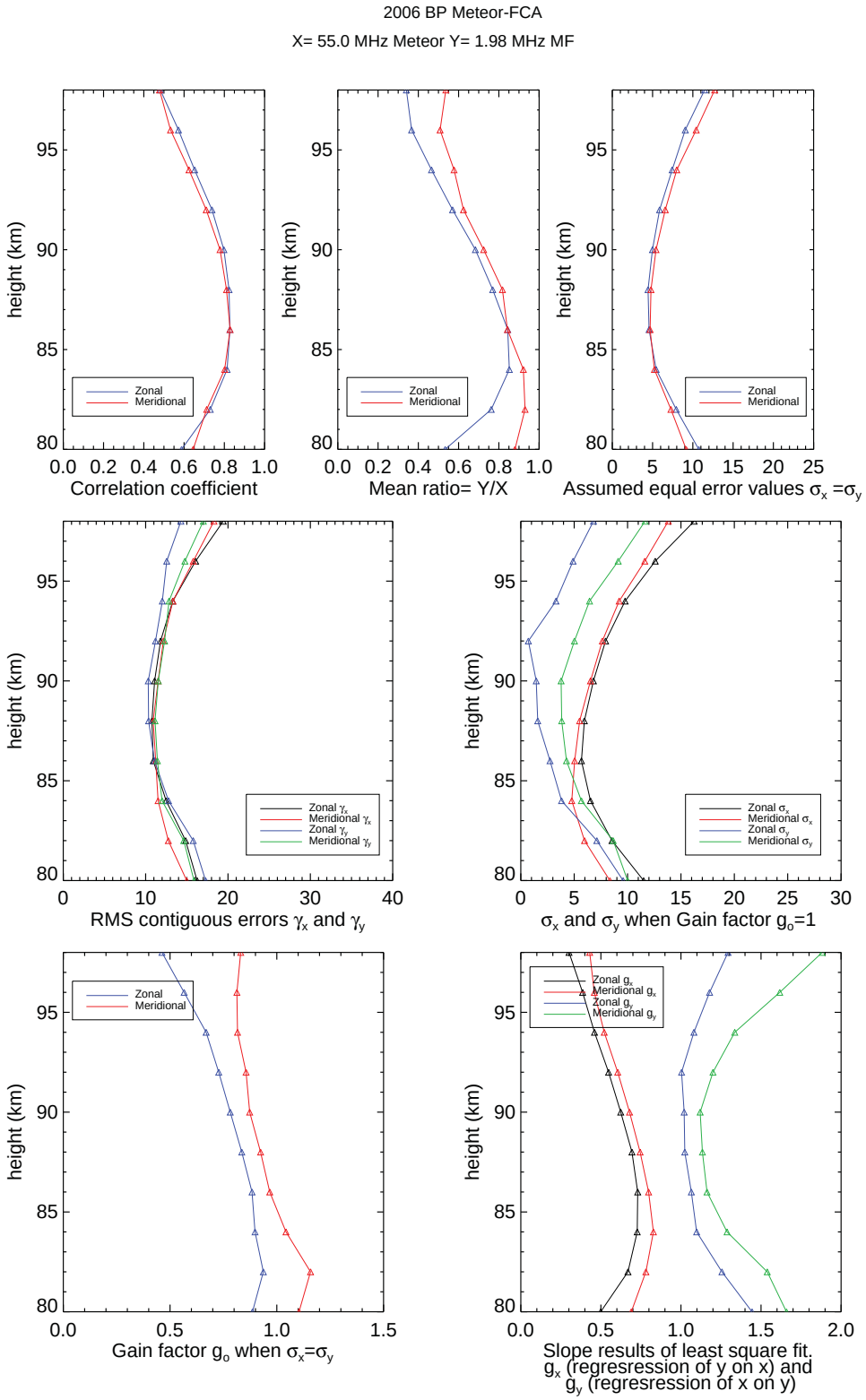

Figure 7.28: Scatter plot summary for 2006 BP 55 MHz meteor and MF FCA comparison.

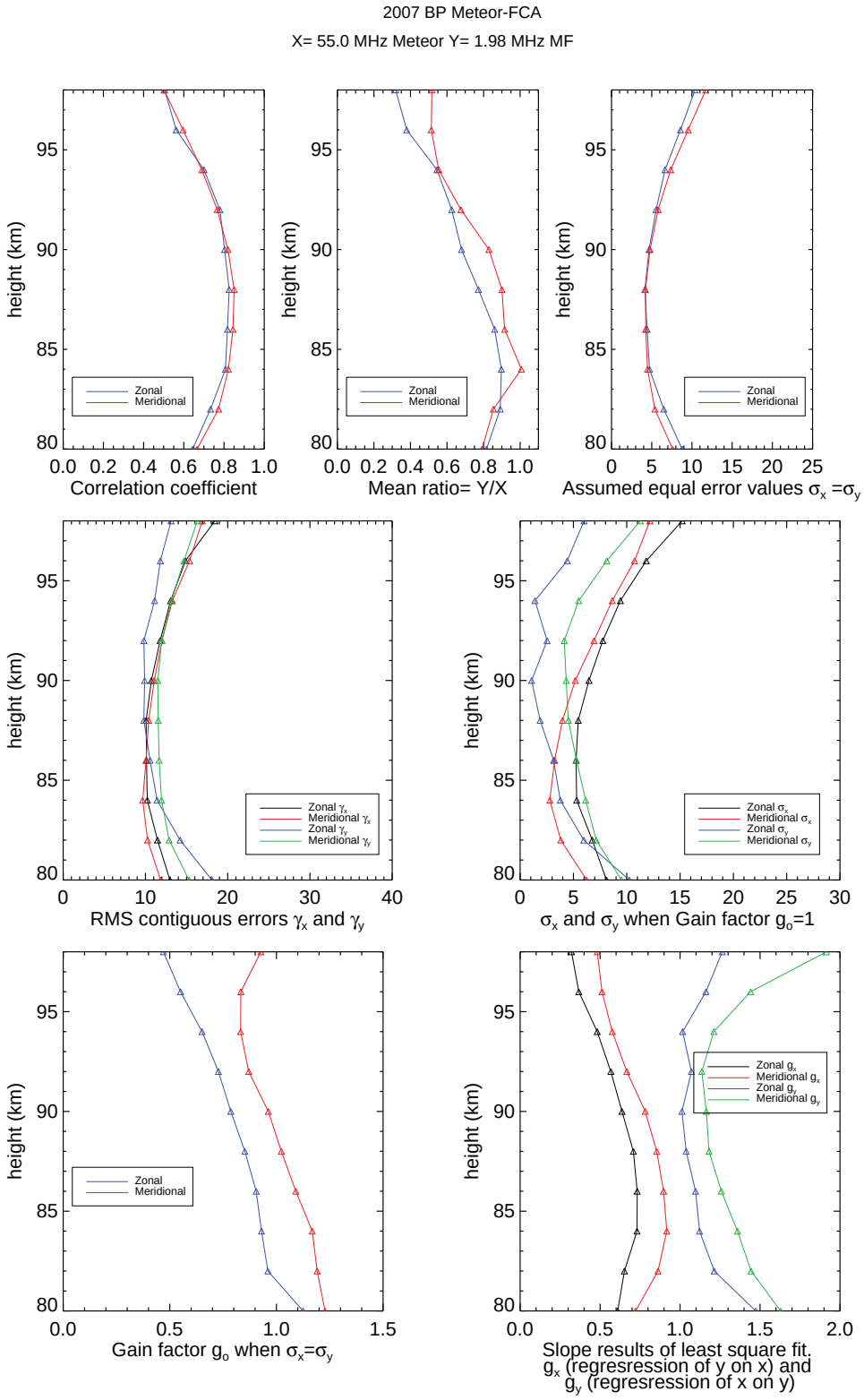

Figure 7.29: Scatter plot summary for 2007 BP 55 MHz meteor and MF FCA comparison.

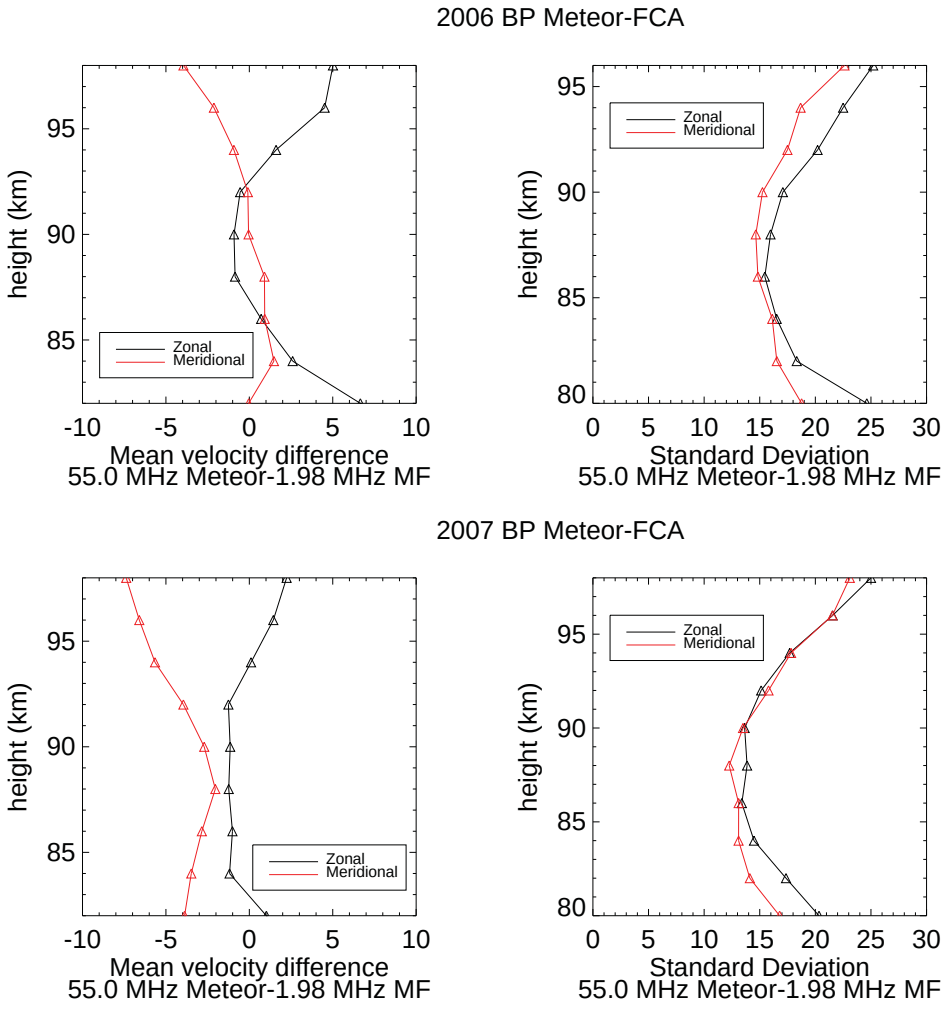

Figure 7.30: Histogram analysis summary for BP 55 MHz meteor and MF FCA.

IDI data for BP was only available for 2007 for comparison with meteor winds. For a full description of the IDI technique see Holdsworth and Reid [2004a]. In the comparisons between the meteor and the MF IDI winds, it can be seen that there is a consistently high correlation between the two techniques over the majority of the height range. The mean ratio of the IDI to meteor peaks at 1.0 at 86 km and is also quite high (≥ 0.8) between 80 and 90 km. The results in Figure 7.31 are very similar to that of meteor FCA comparison. The mean difference between IDI and meteor winds was determined for all heights using the histogram analysis technique and the results can be seen in Figure 7.32. The mean differences were on average larger than those of the corresponding meteor FCA comparison despite showing similar correlative statistics to the 2007 meteor-FCA comparison. The mean differences and standard deviations of the differences from the histogram analysis are only slightly larger than those found in the comparison of meteor and IDI winds by Jones et al. [2003]. It is difficult to directly compare the two results as the histogram analysis was performed on the wind speed rather the zonal and meridional components. Previous comparisons between meteor and MF SA winds (e.g. Cervera and Reid [1995]; Hocking and Thayaparan [1997]) have suggested that wind estimates from MF radar above 90 km tend to underestimate the meteor velocities. Figures 7.33 and 7.34 indicate that this is in fact dependent upon season. This result agrees with what was found by Jones et al. [2003] where it is suggested that the differences between meteor and MF velocities depend upon season, levels of gravity wave activity and system configuration. Figure 7.35 appears to support this suggestion to a degree. It can be seen that in fact the meteor underestimates the MF during certain times of the day at certain heights. The plots in Figure 7.35 are not definitive as the meteor data used in the analysis was only available from 29/01/2007 to 30/08/2007, the majority of which was mainly toward the end of the the period due to technical issues with the radar.

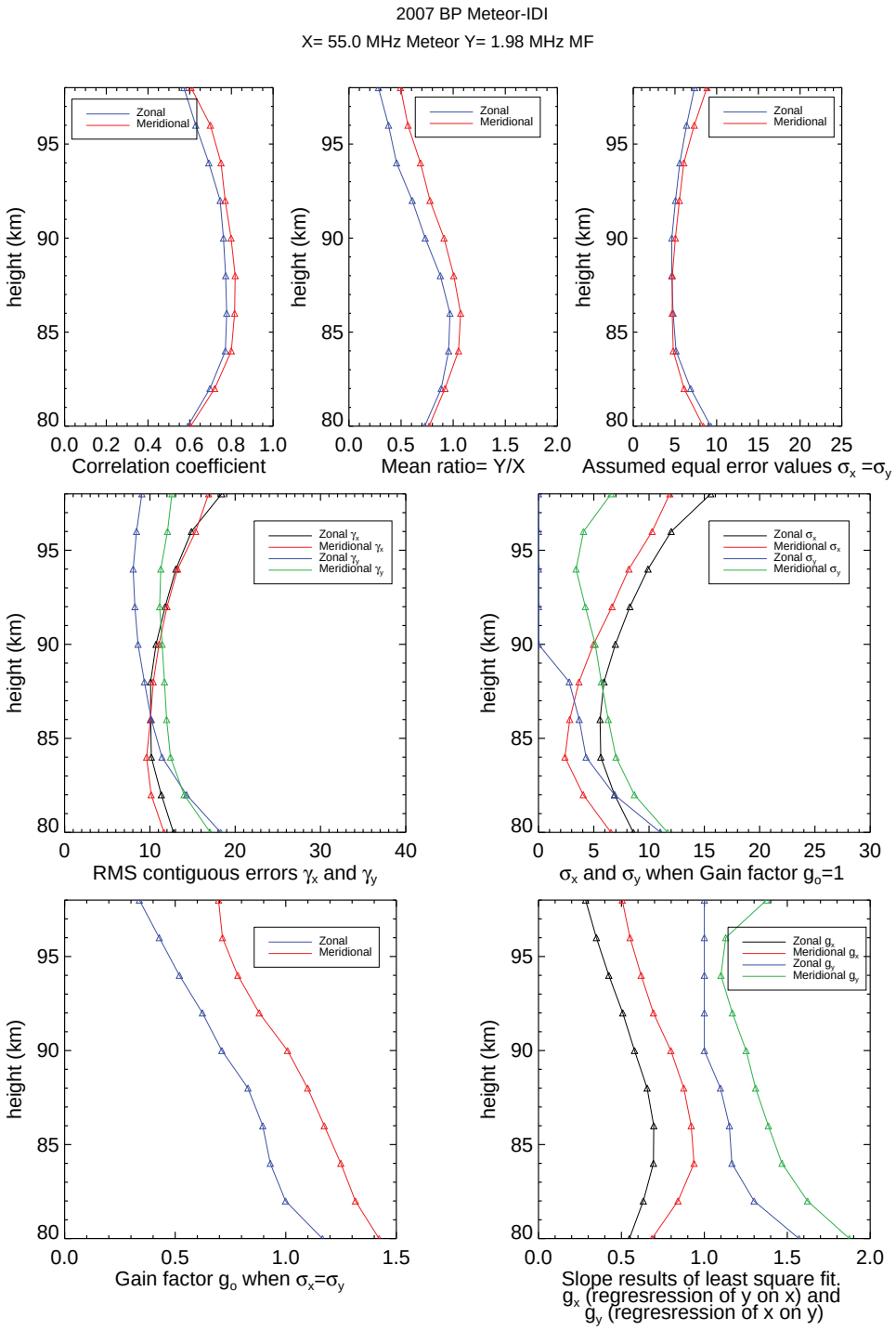

Figure 7.31: Scatter plot summary for 2007 BP 55 MHz meteor and MF IDI comparison.

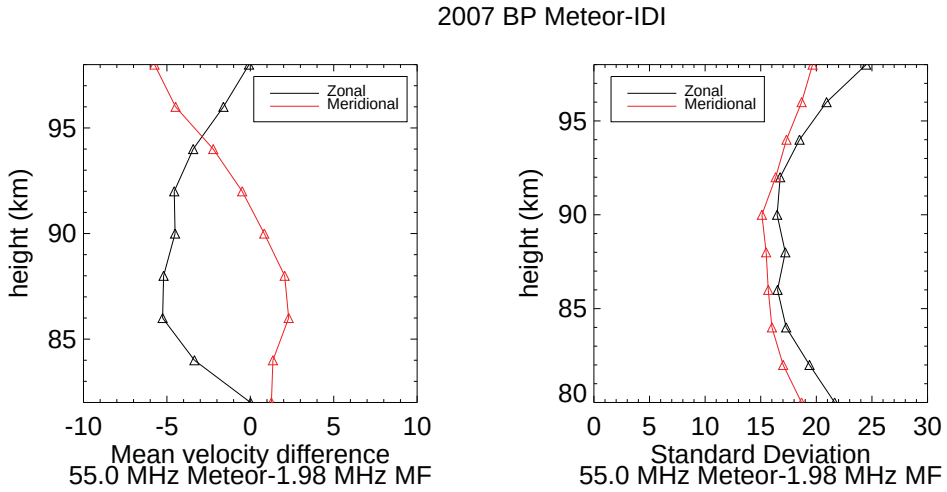

Figure 7.32: Histogram analysis plot summary for 2007 BP 55 MHz meteor and MF IDI comparison.

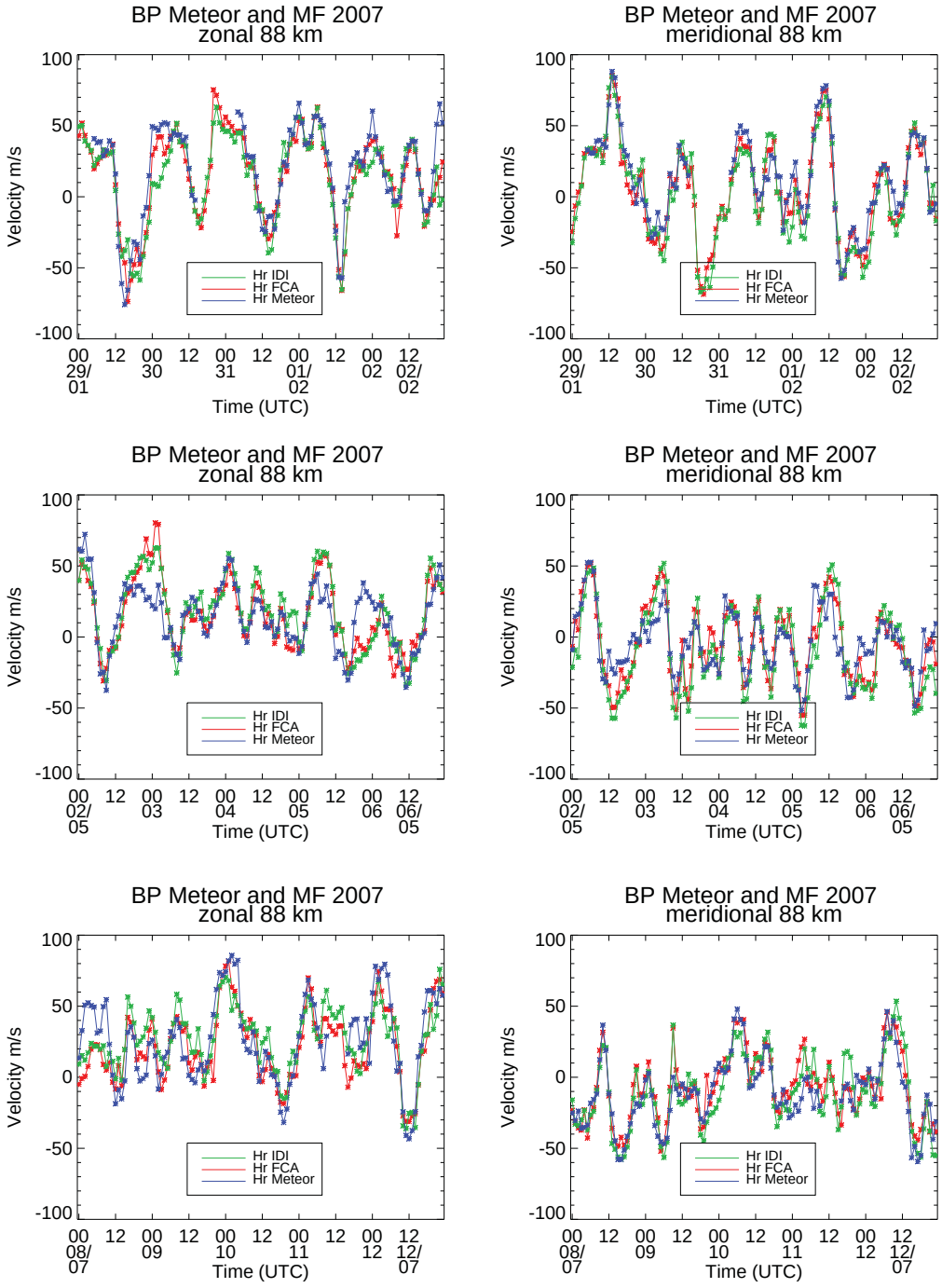

Figure 7.33: 2007 BP meteor and MF velocities at 88 km. Below 90 km the MF winds agree with the meteor winds, however there are instances where the meteor underestimates the MF winds and vice versa.

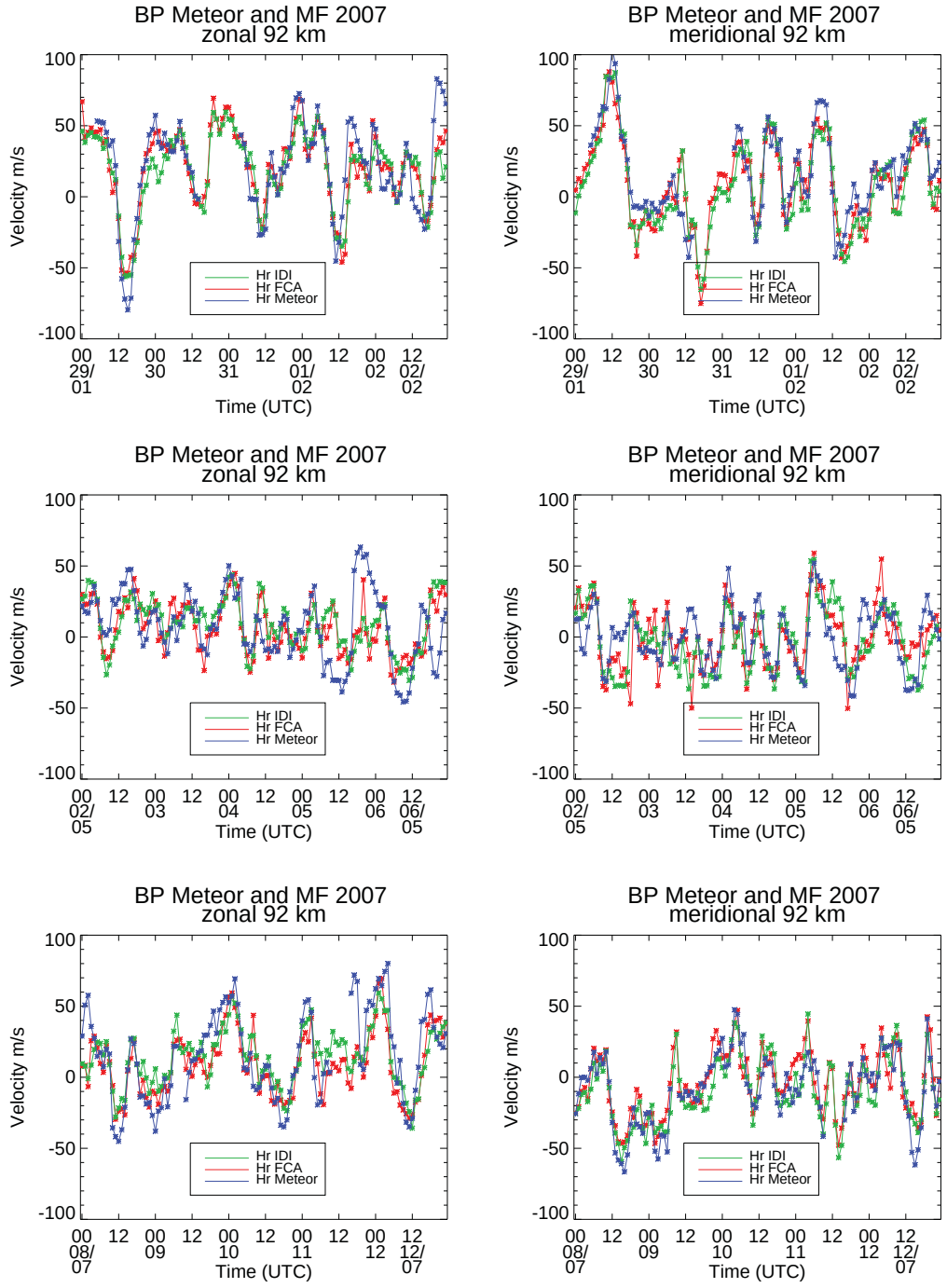

Figure 7.34: 2007 BP meteor and MF velocities at 92 km. Above 90 km it is more apparent that the MF winds underestimate the meteor winds, however there are instances where the meteor winds underestimate the MF winds.

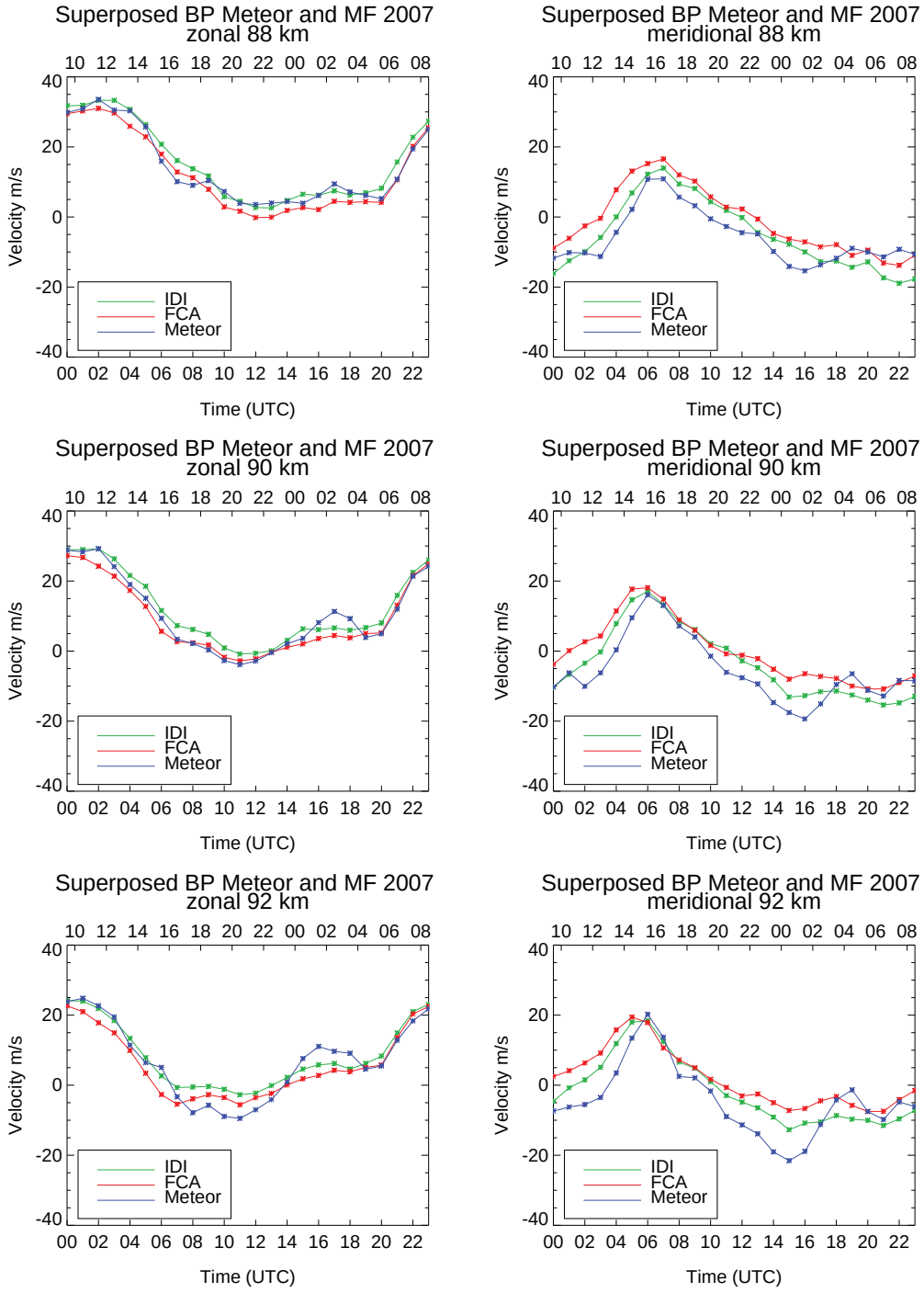

Figure 7.35: 2007 BP meteor and MF superposed wind velocities. The top axes are local time stamps. There is no clear cut case of the MF winds underestimating the meteor winds at certain times of the day and vice versa. This would suggest that the number of meteor echoes or scatterers in the case of the MF is only part of the story and that there are in fact other factors which contribute to the observed underestimations. The times when each technique underestimates the other appears to coincide with periods of the day where minimal scatterers are available for that technique.

7.5 Summary

In this chapter there were several long term comparisons presented of mesospheric wind measurements made between different radar systems and different techniques for observing the wind field. A unique comparison of winds measured between two co-located meteor radars along with comparisons between meteor radar observations and MF radar observations were presented. While the latter comparison has been performed on several occasions, the co-location of the three instruments at Davis provided a pathway for further understanding the differences between winds estimated by both techniques. The three systems served to reduce the number of unknowns in the regression analysis (i.e. σ_x, σ_y or g_0) and hence further clarify and quantify the statistical relationship between the meteor and MF techniques.

Comparisons between meteor and both MF O-mode and X-mode observations have served to highlight the quality of wind estimates of different polarisation modes for MF radar observations. The extended comparisons have shown correlations and mean ratios of between 0.6 and 0.8 for the meteor and MF O-mode comparison below 90 km and decreasing thereafter. Typically the best agreement occurs at approximately 86 km where both meteor and MF O-mode observations are considered to be optimal. The meteor and MF X-mode comparisons along with the MF O-mode and X-mode comparisons clearly show correlations between 0.5 and 0.7 at 80 km and gradually decreasing thereafter. This clearly indicates that some prudence is required when utilizing X-mode wind estimates for comparisons. Comparisons between meteor and MF winds at Davis have served to highlight a difference in the quality between zonal and meridional components of the wind estimates. While this feature appears to be common amongst the comparisons made, it is believed that the use of linear receive antennas at Davis has served to slightly enhance this due to the variation in antenna gain and meteor flux with azimuth. This is more evident with the Davis 55 MHz meteor comparisons due to the interleaved experiment sequence run on that radar and typically the lower echo rates associated with meteor observations made at 55 MHz compared with observations made at 33.2 MHz. Although echo rate is a major contributor to the quality of meteor wind estimates over the height range of the meteor distribution, other factors such as scattering mechanisms, sampling of wave motions, system configuration and seasonal variations are believed to play a strong part in the quality of these estimates. Overall there

is generally good agreement though between directions determined by both techniques.

Comparisons of winds between meteor and MF radar at Buckland Park have been made previously [Cervera and Reid, 1995], however new light has been brought upon the subject through the use of a high-powered meteor radar system. The high-powered system has improved daily echo rates and served to help improve the statistical reliability of wind estimates at heights outside the peak height through an increased number of samples in time-height bins. The meteor and MF FCA comparison as well as the meteor MF IDI comparison show similar correlative and mean ratio results that were observed the Davis meteor and MF O-mode comparison. Correlations and mean ratios were between 0.6 and 0.8 maximizing at approximately 86 km and there was generally good agreement between directions overall. While it is accepted that MF winds generally underestimate meteor winds at heights greater than 90 km, the comparisons between meteor and MF O-mode winds at Davis and in particular the comparisons between meteor and MF FCA and IDI winds at BP have shown that there are in fact instances where the meteor winds underestimate the MF winds above this height. The superposed wind analysis performed between the BP meteor, FCA and IDI winds, indicates times in the 24 hour period where underestimation occurs with the meteor winds compared with the MF winds and vice versa. This phenomena approximately coincides with periods where minimal scatterers are available for the technique. This is not conclusive due to the limited availability of meteor data and the fact that most of it was available toward the end of the observation period, however there is a strong indication none-the-less. Overall it was observed that a bias of between 10 to 20% exists at 86 km depending upon the MF technique used in the comparison between the meteor and MF radar, however this increases as we look at heights further away from the optimum height ($\sim$86 km) for both meteor and MF observations.